KTH Industrial Engineering
and Management

Thermodynamic database for Zirconium Alloys

ROSA JERLERUD PÉREZ

Doctoral Thesis

School of Industrial Engineering and Management
Department of Material Science and Engineering
Royal Institute of Technology
SE-100 44 Stockholm, Sweden
2006

Akademisk avhandling som med tillstånd av Kungliga Tekniska Högskolan i Stockholm framlägges för offentlig granskning för avläggande av teknologie doktorsexamen måndag den 24 april 2006, kl. 10.00 i sal F3 Lindstedsvägen 26, Kungliga Tekniska Högskolan, Stockholm

---

ISRN KTH/MSE--06/03--SE+THERM/AVH
ISBN 91-7178-308-3

Rosa Jerlerud Pérez, Thermodynamic Database for Zirconium Alloys

School of Industrial Engineering and Management
Department of Material Science and Engineering
Royal Institute of Technology
SE-100 44 Stockholm, Sweden

ISRN KTH/MSE--06/03--SE+THERM/AVH
ISBN 91-7178-308-3

"Para desembarcar en la isla de la sabiduria hay que navegar en un oceano de aflicciones"

Sócrates

Abstract

For many decades zirconium alloys have been commonly used in the nuclear power industry as fuel cladding material. Besides their good corrosion resistance and acceptable mechanical properties the main reason for using these alloys is the low neutron absorption.

Zirconium alloys are exposed to a very severe environment during the nuclear fission process and there is a demand for better design of this material. To meet this requirement a thermodynamic database is useful to support material designers.

In this thesis some aspects of the development of a thermodynamic database for zirconium alloys are presented. A thermodynamic database represents an important facility in applying thermodynamic equilibrium calculations for a given material providing: 1) relevant information about the thermodynamic properties of the alloys e.g. amount and composition of phases, oxygen activity, heat capacity etc, and 2) significant information for the manufacturing process e.g. heat treatment temperature.

The basic information in the database is first the unary data, i.e. pure elements; those are taken from the compilation of the Scientific Group Thermodata Europe (SGTE) and then the binary and ternary systems. All phases present in those binary and ternary systems are described by means of the Gibbs energy as a function of composition and temperature. Many of those binary systems have been taken from published or unpublished works and others have been assessed in the present work. The elements included in the databse are: C, Fe, Cr, Nb, Ni, Mo, O, Si, Sn, and Zr + H, and the assessment performed under this thesis are: Cr.Sn, Mo-Zr, Sn-Zr, Fe-Nb-Zr and Nb-O-Zr. All the calculations have been made using Thermo-Calc software and the representation of the Gibbs energy obtained by applying Calphad technique with some use of *ab initio* calculations.

Key Words: Zirconium alloys, thermodynamic equilibrium, thermodynamic properties, binary system, ternary system, Gibbs energy, Thermo-Calc, Calphad, binary system, ternary system

Acknowledgments

There are many persons to whom I would like to express my gratitude for all kind of **help and support**, nevertheless if I mention everyone, the list will never end. Acknowledgements are expressed to:

My supervisor B. Sundman for giving me the opportunity to my PhD and also for his guidance, help and his patience during this work and to Mallin Selleby for always being prepared to answer many many questions.

The sponsors of this project, the Swedish nuclear power industry composed by the following groups: Barsebäck Kraft AB, OKG AB, Forsmarks Kraftgrupp AB, Vattenfall AB, Ringhalsverket, Swedish nuclear power inspectorate (SKI), and Westinghouse Electric Sweden for financial and moral support.

Many people who were at the department of material science in the beginning of my studies gave me a hand during moments of doubt and confusion. I will always be grateful to Lars, Susane, Malin Ekroth, Åsa, Mikus, Sandra etc, Also I would like to thanks Hans Bergqvist for shearing with me all his knowledge about Zr alloys.

Especial gratitude are also extended to Nathalie Dupin and the late Himo Ansara and to all my co-authors Jean-Marc, Caroline, Vitaly and Pavel for all help, advises, fruitful discussions and for a very instructive and very nice time working together.

My family, in Venezuela, my sister Gladys, my mother Elba, my father Antonio and my brothers Frank Jesús and my late brother Hugo, who have always played a very important roll in my life and in early stage materially supported my studies and gave me confidence and love.

My other family here in Sweden, my two wonderful children: Sebastian and Diana and my dear husband Michael for keep giving me love and understanding and also my gratitude is extended to my mother in-law and my father in-law.

My friends Henrry, Ana Iris, Antonio, Cheo for all their support and Dennis Andersson for reading this manuscript.

Preface

This thesis is comprised by the following papers:

I Thermodynamic Assessment of the Cr-Sn binary system
Rosa Jerlerud Pérez and Bo Sundman
Calphad, Vol. 25, No. 1 (2001) pp.59-66
ISRN KTH/MSE--06/04--SE+THERM/ART

II Thermodynamic assessment of the Mo-Zr binary phase diagram
Rosa Jerlerud Pérez and Bo Sundman
Calphad, Vol. 27 (2003) pp. 253-262
ISRN KTH/MSE--06/05--SE+THERM/ART

III Structural stability of intermetallic phases in the Zr-Sn system
V.I. Baykov, Rosa Jerlerud Pérez, P.A. Korzhavyi, B. Sundman and B. Johansson
Submitted to Scripta Materialia
ISRN KTH/MSE--06/06--SE+THERM/ART

IV Contribution to the study of phase equilibria in Fe-Nb-Zr and preliminary thermodynamic assessment at 800 °C
R. Jerlerud Pérez and B. Sundman
To be submitted to Journal of Nuclear Materials
ISRN KTH/MSE--06/07--SE+THERM/ART

V Thermodynamic evaluation of the Nb-O-Zr system
R. Jerlerud Pérez and A.R. Massih
Submitted to Journal of Nuclear Materials
ISRN KTH/MSE--06/08--SE+THERM/ART

VI The Sn-Zr binary system: experiments and thermodynamic assessment
R. Jerlerud Pérez, C. Toffolon-Masclet, J.-M.Joubert and B. Sundman
To be submitted to Journal of Phase Equilibria
ISRN KTH/MSE--06/09--SE+THERM/ART

Table of contents

Chapter 1
Introduction

The knowledge of equilibrium phase diagram for multicomponent systems is very helpful for processing advanced materials. Since phase diagrams are defined from the thermodynamic properties, computer aided modelling of theses properties constitute the basis of the thermodynamic database in alloys design. The models describe the thermodynamic properties of many types of phases, by parameters that uniquely determine the properties of various phases and are then stored in databases. Such parameters must be assessed using the available theoretical and experimental data. A thermodynamic assessment makes use of the CALPHAD (CALculation of Phase Diagram) technique, where the models are expressed in term of mathematical expressions, with parameters that are optimised to reproduce the reality by comparing the available experimental information with the same information calculated from the models. The experimental information includes both the phase equilibria (phase diagram information) and thermochemical data. However, themodynamic data is often not available in literature, in such case other sophisticated methods have to be consulted in order to replace the missing information. Such methods are based on Quantum Mechanic Calculation [60,61] or Miedema approach [62] for the enthalpy of formation of intermetallic compounds.

The great advantage of the CALPHAD techniqe is that it is able to predict thermodynamic properties of higher order systems from those of lower order binary and ternary systems. Such an approach provides a powerful tool as information from binaries and ternaries can be directly used to predict multicomponent alloys behaviour.

In this thesis the basis for a thermodynamic database for Zirconium alloys has been developed with the following components: C, Fe, Cr, Nb, Ni, Mo, O, Si, Sn, and Zr + H, and the thermodynamic description of following binary and ternary systems: C-Zr, Cr-Sn, Cr-Fe, Cr-Nb, Cr-Ni, Cr-Zr , Fe-Nb , Fe-Ni , Fe-Sn, Fe-Zr , Ni-Sn, Ni-Zr, Mo-Zr, Mo-Ni, Mo-Si, Nb-Sn, Nb-Zr, Si-Zr, Sn-Zr, Fe-Nb-Zr, Cr-Ni-Zr, Cr-O,Ni-O, Cr-Ni-O, Cr-Fe-O, Fe-O, Fe-Ni-O, O-Sn, O-Nb, O-Nb-Zr ,O-Zr and H-Zr. Those systems have been taken either from literature, from unpublished works or assessed by this author. In

this thesis thermodynamic assessment of Cr-Sn, Mo-Zr, Sn-Zr, Fe-Nb-Zr has been performed using the Parrot module of the Thermo-Calc software. The thermodynamic description of the Nb-O-Zr was verified from binary extrapolations. Additionally, a contribution to improve the thermodynamic knowledge of the Sn-Zr binary system has been done by experimentally studying some aspect on the phase equilibria in this system and theoretically creating data (quantum mechanic calculations) on the enthalpy of formation of the intermetallic compounds.

The aim with this work is to provide a database for prediction of thermodynamic properties of the Zr multicomponent and multiphase alloy in order to reduce the amount of experimental work necessary to test and develop new alloy compositions, helping for example to select temperatures for heat treatment. However, this task can not be completely achieved without further work on the thermodynamic description of other important ternary systems where Zr is the third component interacting with the alloying elements, for example Cr-Fe-Zr, Fe-Ni-Zr, Fe-Sn-Zr, O-Sn-Zr etc.

1.1 Introduction to Zirconium and its alloys

Zirconium is a transition metal found in group IVB (Ti, Zr and Hf) of the periodic table and has atomic number 40. In nature it is commonly found associated with hafnium. The main sources of zirconium are the minerals zircon $(Zr,Hf)SiO_4$ and baddeleyite, $(Zr,Hf)O_2$. Pure Zirconium is very reactive but corrosion resistant as it reacts with oxygen in the atmosphere to form a protective oxide film that prevents further corrosion of the metal as well it alloys. Zirconium in the form of metal dust can ignite in air at high temperature, even some of its alloys behave likewise

Zirconium has wide industrial applications at the due to the fact that it is un-attacked by any acid except hydrofluoric acid, hence chemical industry take advantage of this property for piping in corrosive environments. In vacuum tubes, it can be used as a purifier i.e. a getter due to its high affinity to oxygen. In metallurgy zirconium oxide (ZrO_2) is used as furnace lining material and as electrolyte. In other fields like medicine it is used for artificial joints and limbs in human bodies.

However the main application field of Zirconium and its alloys is the Nuclear Power Industry. They have been used for the last 50-60 years as design materials for structural components in diverse nuclear reactors, mainly due to their low neutron absorption cross section. A few zirconium alloys has been designed for nuclear application, some of them are shown in Table 1.

The most harmful trace elements found in zirconium alloys are Hf, H and N. Hafnium is an impurity coming from the raw material and increases the neutron capture cross section of the alloy, hence it has to be removed from the raw material before alloy manufacture. Nitrogen may come from the ore processing zirconium/hafnium separation. Hydrogen pick up by the material leads to formation of hydrides which results in hydrogen embritlement. The hydrogen content specifications in the raw material are very strict, however it is easily picked up by Zr during the metallurgical processing of the tubes (fuel containers) and also inside the nuclear reactor.

1.2 Main application field of Zirconium alloys

Nuclear reactors are of various types, among them the Light Water Reactors (LWR), are most common in Europe including Sweden. In LWRs both the moderator[1]

Table 1- Composition range of zirconium alloys, from ASTM (American Society for Testing Materials standards)

Alloying element (mass %)	*Zircaloy-2*	*Zircaloy-4*	*Zr-Nb*	*Zirlo*
Sn	1.2-1.7	1.2-1.7	-	0.96-0.98
Fe	0.07-0.2	0.18-0.24	-	0.0094-0.015
Cr	0-05-0.15	0.07-0.013	-	0.0079-0.0083
Ni	0.03-0.08	-	-	-
Nb	-	-	2.4-2.8	1.02-1.04
O	*	*	0.09-0.13	0.09-0.12

* Usually 1000-1400 ppm

and the coolant[2] are water. Depending on whether water is allowed to boil or not the LWRs are divided in boiling water reactor (BWR), Fig 1, and pressurised water reactor (PWR), Fig 2. Other variants of water reactors exist, like for example the Canadian CANDU (CANadian Deutrium Uranium), in which both coolant and moderator are heavy water. Other kind of reactor systems are for example the graphite moderated reactors which use water as coolant, for example the Russian RBM (boiling water reactors . Core structural parts in PWRs and BWRs are fabricated from zircaloy-2 or zircaloy-4. In BWRs Zircaloy-2 is used for example in fuel cladding and for calandria[3] tubes in CANDUs while Zircaloy-4 is used for both fuel cladding and fuel channels in PWRs and for fuel cladding in CANDUs. The binary alloys Zr-2.4Nb are mainly used for pressure tube materials in the Russian RBMK reactor design.

In order to meet better in-reactor performance, due to their superior corrosion and irradiation stability [1,2] the niobium bearing multicomponent Zr alloy Zirlo [4], and

[1] Moderator is a material used to slow down the extremely energetic neutron produced during nuclear fission. A characteristic moderator materials are, water, heavy water and in some kinds of reactor use graphite.

[2] The coolant is the substance used to remove the heat generated in the reactor, usually light water is used as coolant but depending on the power plant design also heavy water, liquid metals (Na and K) or even gases ($C0_2$) are used.

[3] The pressure-tube-tank design in CANDU

[4] Zirlo is a registered trademark of Westinghouse Electric Corporation

its Russian equivalent E-365[5] were developed as an alternative cladding material for Pressurized Water Reactor (PWR) and for the Russian RBMK pressure tubes [1] respectively.

The nuclear fuel UO_2 is placed in a long zirconium alloys tubes forming the fuel rods, but depending on the reactor type the fuel rods are either loaded individually in the reactor or grouped together to form a fuel assembly, see Fig 1.1 for details. Nuclear fission occurs in this part of the reactor and the fuel cladding has the function to hold back the radioactive fission products. Thus, the severe conditions in a nuclear reactor demand very high requirements concerning cladding material properties. Those are summarised as follows:

- Good corrosion resistance (mechanical and chemical stability with the nuclear fuel and the coolant, for example, water in BWR).
- Good high-temperature mechanical strength, e.g. high resistance to deformation caused by the thermally expanding UO_2
- Favourable nuclear properties (low neutron absorption cross section, from neutron efficiency point of view this is the most important of all).

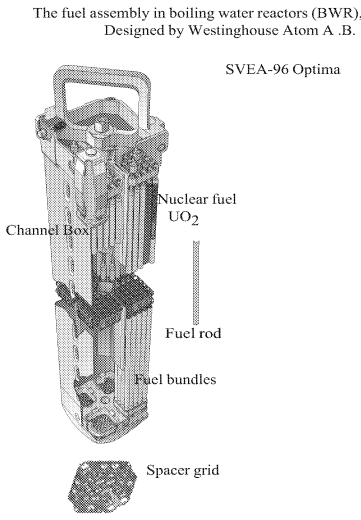

FIG.1.1 Fuel Assembly in BWR, designed by Westinghouse Electric Sweden…

Regarding reactor core materials LWR presents some similarities, however environmental differences between these two kinds of reactors leads to distinctive behaviour of the Zirconium alloys. In the BWR steam is generated inside the reactor, water is allowed to boil, then it goes directly to the generator, see Fig 1.2. In the PWR the

[5] E-365 design in Russia, Certificate, USSR,No. 64815

steam is generated outside of the reactor in a secondary heat transfer, see Fig 1.3. In this type of reactor boiling is suppressed due to the high in-reactor pressure.

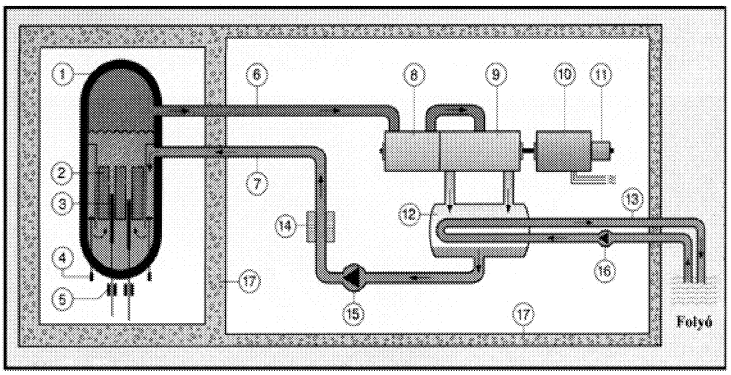

Fig 1.2 BWR, in Ref. [3] 1 Reactor pressure vessel; 2 Fuel rods; 3 Control rod; 4 Circulating pump; 5 Control rod drive; 6 Fresh steam; 7 Feedwater; 8 High pressure turbine; 9 Low pressure turbine; 10 Generator; 11 Exciter; 12 Condenser; 13 Cooling water; 14 Preheater; 15 Feedwater pump; 16 Cooling water pump; 17 Cooling water pump.

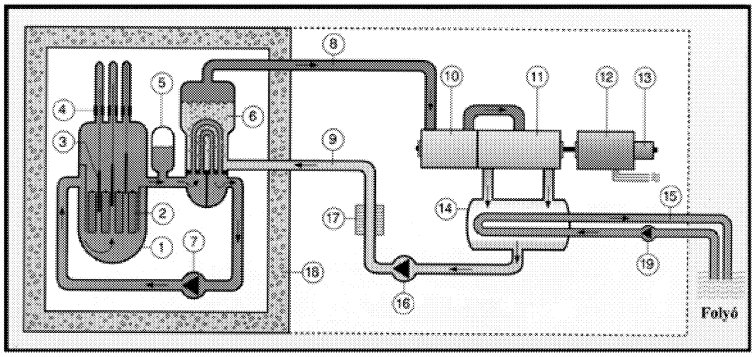

FIG 1.3 PWR in Ref. [3] 1 Reactor vessel; 2 Fuel elements; 3 Control rods; 4 Control rod drive; 5 Pressurizer; 6 Steam generator; 7 Main circulating pump; 8 Fresh steam; 9 Feedwater; 10 High pressure turbine; 11 Low pressure turbine; 12 Generator; 13 Exciter; 14 Condenser; 15 Cooling water; 16 Feedwater pump; 17 Feedwater pre-heater; 18 Concrete shield; 19 Cooling water pump.

1.3 Alloying elements and microstructure

Zirconium has two allotropic modifications, the α-Zr phase with hexagonal closed-packed structure (HCP) which is stable up to 863 ºC. Above this temperature the β-Zr phase with a body centered cubic structure (BCC) is stable. The alloying elements have different solubility in the α-Zr and β-Zr. Oxygen is an α-Z stabilizer, i.e. expands the α-Zr phase field. Oxygen dissolves interstitially in the α-Zr phase and in controlled amounts it increases the yield strength by solution hardening. According to the ASTM standard the oxygen content in zircaloy must not exceed 1400 ppm. Tin is also an α-Zr stabilizer. It dissolves substitutionally in the matrix and the purpose of its addition is to achieve a solution hardening. The rest of alloying elements have larger solubility in β-Zr, they are β-Zr stabilizers. Due to their low solubility in α-Zr, they precipitate as secondary phase particles (SPP) in the matrix material. Addition of Nb are believed to have an effect in the corrosion resistance [1,2,4] as well the creep strengh [15].

The main steps in the Zr alloys fabrication are summarised in the following schema:

Stage	*Operation*
Multiple Melting	Vacuum-arc melting
Hot working	Heating to β range→ quench
	Hot extrusion in upper α range
Cold working and annealing	Cold rolling
	Annealing in upper α range
	Cold rolling
	Annealing in upper α range
	Final cold rolling
	Final annealing ~575°C
Final	Stress realise annealing

During the fabrication multiple arc meltings is carried out in order insure homogeneous distribution of the alloying elements. Due to zirconium's high affinity to oxygen vacuum has to be conserved during melting as well as in the annealing furnaces. Heating to the β phase range and quenching has the purpose to dissolve coarse SPP in order achieve a fine precipitate. The size distribution of these particles is important for strength as well as for corrosion resistance [5]. Hot extrusion in the in upper α range does not give significant particle growth and after the final rolling the particle are a few μm in size. During cold rolling (in pillger mills) the material grains acquires preferred orientation (texture).

The microstruture of the Zircaloys depend on the heat treatment. The recrystallized matrix of theses alloys consist of equiaxed grains of α-phase with SSP precipitated both within the grain and at the grain boundaries. The microstructure of the Zircaloy transformed from the β-phase consists of Widmanstätten α plates. However depending on the quenching rate and β-grain size prior to quenching this microstructure can exhibit several morphological differences, for example the basket-weave (intersecting short plates within the grains and parallel plates [6] growing from the grain boundary of the parent β phase). The basket weave microstructure has been associated with the

presence of impurities in the material, for example C and Si [7] and small grain size of the parent phase. The parallel plates are associated with larger grain size. The matrix of the zircaloys contains Sn and O in solution e.i. α-Zr. The secondary phase particles are the ternary compounds: $Zr(Cr,Fe)_2$ and $Zr_2(Fe,Ni)$. The $Zr(Cr,Fe)_2$ particles belong to Laves phase family. They crystallize into three modifications: the $MgZn_2$ (C14) or the $MgNi_2$ (C36) type structure, both with a hexagonal lattice and $MgCu_2$ (C15) type structure with a cubic lattice. The laves C15 and C14 are common in Zircaloy-2 and zircaloy-4. Those compounds are based on the binary compounds $ZrFe_2$ and $ZrCr_2$, see Fig 1.4 and Fig 1.5.

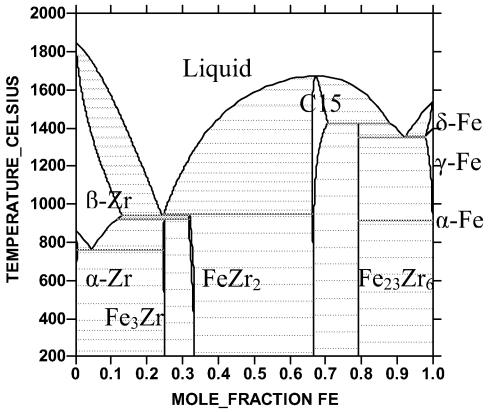

FIG 1.4 Fe-Zr binary phase diagram by Servant *et al.* [74]

The precipitation of the SPP depends on the alloys composition, at certain Fe/Cr ratio the Laves phase forms, as this ratio increases a Zr richer phase $FeZr_3$ precipitates besides laves phase.

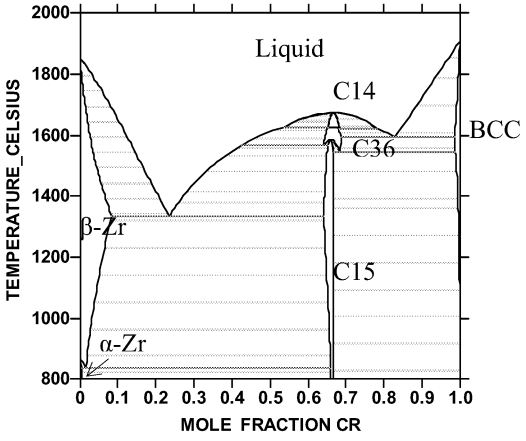

FIG 1.5 Cr-Zr binary phase diagram by [71]

It has the BRe_3 orthorombic prototype structure. The ternary compound $(Fe,Ni)Zr_2$ C16 has the Al_2Cu tetragonal prototype structure and belongs to the family of Zintl compounds. This tetragonal C16 phase precipitates as SPP in zircaloy-2 and is also found in the binary Zr-Fe and Zr-Si.

Zirlo[6] (Zr-1Nb-1Sn-0.5Fe) and M5[7] together with the similar Russian alloys E635 (Zr-1.2Sn-0.4Fe-1Nb) and E110 respectively [8,9,10], are the new generation of Nb modified alloys. These alloys have shown superior properties, for example better corrosion resistance and lower irradiation growth. This makes longer exposure possible and satisfies the demanding operation conditions for higher fuel burn up. The microstructure of fully recrystallized Nb containing multicomponent Zirconium alloy Zirlo and E365 consist of very small β-Nb particle of ~50nm that precipitated in the α-Zr matrix. The secondary phase particles are the ternary $Fe_2(Nb,Zr)$ C14 an the Fe $(Nb,Zr,)_2$ with a structure of $TiNi_2$ cubic prototype structure [1,2, 8-10, 11-14]. In the matrix, some Nb is dissolved in the α-Zr- solid solution.

1.4 Texture

The pure Zirconium has a hexagonal crystal lattice with a characteristic direction, the basal plane normal (the basal pole) [0001]. This special feature in the metal results in a marked anisotropy and deformation occurs both by slip and twinning.

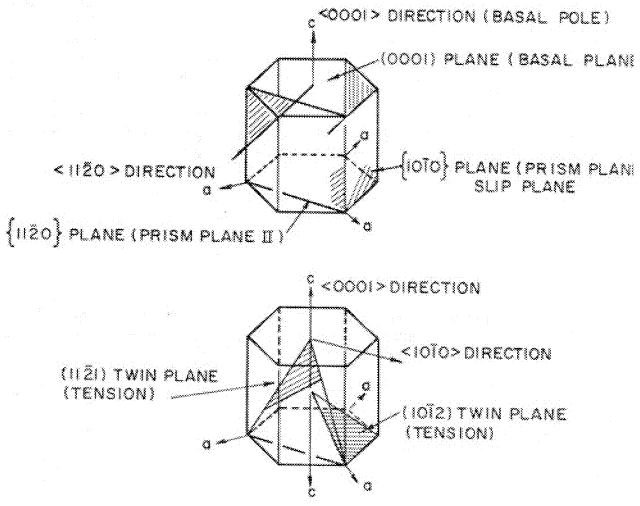

FIG. 1.6 Deformation system in Zr

[6] Westinghouse trade Mark
[7] Zr1NbO alloys (French Trade Mark)

At room temperature slip occurs mainly on prism plains in the **a** direction: $\{10\bar{1}0\}\langle 1\bar{2}10\rangle$ system or on the basal plane {1011} (0001). A higher deformation and higher temperature **c+a** (pyramidal) types is activated on $\{11\bar{2}1\}$ or $\{10\bar{1}1\}$ planes. At low temperatures and under **c** axis compression Zr deforms by twinning: {1011} <1123>. On tension the {1012} <1012> system operates [15], see Fig. 1.6. Thus under stress or compression the [0001] is a strong direction of the crystal, this preferred orientation (texture) of the grains brings the anisotropy of single crystal into the polycrystalline Zr alloys. Since the matrix of Zr alloys is the hcp phase α-Zr, the material has the same peculiar characteristics as the pure metal. During manufacturing of the zircaloy rod the basal pole of the hexagonal lattice is tilted ~30° from the normal of the tube towards the tangential direction which develop the pronounced crystallographic texture.

Chapter 2

"In-reactor" Zirconium alloys performance

Nuclear reactors are very powerful and complex engines, within which many parameters have to be taken care of to insure high security levels. Some of the important physical properties of nuclear reactor components, for example creep and growth, corrosion, fracture toughness, hydrogen uptake can change as a result of microstructure evolution during materials in-reactor performance.

Inside the nuclear reactor, zirconium alloys are exposed to a very complex and harmful environment that jeopardise the integrity of the material. First of all, irradiation, due to neutron flux, cause micro-structural changes, for example irradiation growth and creep on the cladding material. The SPP undergo amorphization and eventually dissolve. The type of SPP morphology and their distribution affect the materials "in reactor" performance, especially the corrosion resistance. Hydrogen, which arises from the water used to remove the heat of the fuel rod, causes hydrogen embritlement. Hydrogen may also pick up during the manufacturing of the tubes. Stress corrosion cracking, is another serious problem. All this together contribute to the degradation of the materials properties.The purpose of this chapter is to give an idea of some thermodynamic influences of the material behaviour during operating conditions.

2.1 Secundary phase particles (SSP) *in- reactor* behaviour

Due to the low solubility of Fe, Cr, Ni and Nb in α-Zr, they precipitate as secondary phases particles (SPP) in Zr alloys. Some of these SPP undergo substantial changes in reactor such as size distribution, composition and crystal structure. Irradiation causes the atoms to leave their place in the crystal lattices by nuclear collisions, and a crystalline to amorphous transformation is induced. It has been commonly observed that the intermetallics $(Fe,Cr)_2Zr$ and $(Fe,Ni)_2Zr$ in Zircaloy-2 and Zircaloy-4, became amorphous and lose a large fraction of Fe. Depending on the irradiation type (neutron, ion or electron) and conditions (temperature and irradiation doses) and the particle type,

they behave differently. The SPP may become completely amorphous, develop a duplex structures (crystalline core surround by an amorphous ring) or even remain crystalline. In the second case amorphous transformation begins at the particle matrix interface and advance inwards until complete amorphization is accomplished [16,17,18]. Dissolution and re-precipitation of the particles may take place [23]. The crystalline to amorphous transformation of intermetallic compounds under neutron, ion and electron irradiation has been widely studied. It has been observed that doses to amorphization increases with temperature and that there is a critical temperature above which amorphization can not occur due to the effect of thermal annealing (materials self-repair) [19,20,21]. In Ref. [22] the relevance of the irradiation conditions on tendency for amorphization in intermetallics was studied and it was pointed out that amorphization depends on the materials properties as well on the irradiation condition and the total irradiation dose received by the material. Others factors like compound stoichiometry (the deviation from it), the presence of defects (dislocations, stacking faults, anti-phase boundaries) were also discussed. Regarding dislocations and stacking faults, in the work by [16,18,19] it has been observed in material with such defects the tendency for amorphization is high.

The crystalline to amorphous transformation has been defined as the complete loss of long range crystallographic order, observed in the X-ray diffraction or electron diffraction by the replacement of the spots pattern by ring pattern. Among the many point defects in crystalline solids like intermetallic compounds, anti-site defects play an important role on their stability. Intermetallic compounds often exist in a narrow composition range, deviation from the stoichiometry can be accommodated by anti-site defects or by vacancies, at expense of energy and stability. Under irradiation a great amount of energy is stored in the lattice by the nuclear collitions neutron-atoms, thus the intermetallics are driven away from their equilibrium configurations. A model for amorphization process due to irradiation has been proposed and it states that after amorphization a new meta-stable equilibrium exist between the amorphous phase and the irradiated zirconium matrix. The Fe equilibrium concentration between the amorphous SPP and the irradiated matrix is different from the Fe equilibrium concentration outside irradiation [22,24]. A driving force for this transformation, is given by the contribution due to ballistic mixing between the Fe and zirconium atoms across the matrix-precipitated interface [24] and it was formulated by the modified free-energy criterion in Refs. [22,25].

The amorphization conditions is

$$\Delta G_{irr} \geq \Delta G_{ca} \tag{1}$$

where ΔG_{ca} is the difference in Gibbs energy between the amorphous and unrradiated crystalline state

$$\Delta G_{ca} = G_c - G_a \tag{2}$$

and the ΔG_{irr} is the difference between the free energy of the irradiated and unrradiated crystals considering all kinds od defects in the lattice (poin defect, increase in chemical disorder, stacking faults etc.

In this model is considered that the irradiation induced free energy has two contributions, due to defects increase and the contribution due to the chemical disorder.

Considering the Bragg-Willians description of long-range order, it is possible to evaluate ΔG_{irr} as the change in free energy due to irradiation as:

$$\Delta G_{irr} = \Delta G_{def} + \Delta G_{dis} \tag{3}$$

$$\sum_{j=i,v}(C_i E_i) - T\Delta S_i) + \Delta C_{pab} N\Omega - T\Delta S_{dis} = \Delta G_{irr} \tag{4}$$

where, C_i is concentration of the defect *i,* E_i is the defect formation energy, N total number of lattices sites per mol, Ω is the energy associated with ordering, ΔS_i is the configuraional entropy change due to point defects (in the crystalline phase) and ΔS_{dis} is the chage in the configurational entropy due to anti-site defects (in the crystalline phase). ΔC_{pab} is the change of the A-B pairs bonds per lattice site, it is given by:

$$\Delta C_{pab} = N(A(1-S^2) + B(1-S)) \tag{5}$$

where A and B are constants depending on the crystall structure and S is the Bragg-Willians long-range order parameter [26]

In Fig 2.1 a very simple example is shown to illustrate the presence of anti-site defects in the lattices, and the Gibbs energy of the Fe_2Zr (C15 phase) under usual thermodynamic equilibrium (outside irradiation). The thermodynamic modelling of this phase is made using the Compound energy formalism, CEF, [27,28,29]. It basically defines different crystallographic sites i.e. sublattices , and the Gibbs energy of the phase is determined by the site occupation of the constituents in different sublattices. The C15 phase at reactor operating temperatures is stoichiometric, this mean that Fe and Zr occupied certain fixed sites but at higher temperature the compound is not stoichiometric, which means that a deviation from the stoichiometry can be defined by anti-site defect or vacancies. So the model to represent the Gibbs energy of the C15 phase is schematically written as:

$$(\mathbf{Fe},Zr)_2(Fe,\mathbf{Zr})_1$$

The Gibbs energy of the phase arises from different contributions, the reference Gibbs energy for the pure constituents, the ideal Gibbs energy due to random mixing and the excess Gibbs energy (deviation from the ideal behaviour) as:

$$G_m = {}^{ref}G_m + G_m^{id} + {}^{ex}G_m \tag{6}$$

where ${}^{ref}G_m$ is the reference Gibbs energy which represents a combination of all stoichiometric compounds with one constituent in each sublattice.

$$^{ref}G_m = y^1_{Fe}y^2_{Fe}\,{}^0G_{Fe:Fe} + y^1_{Fe}y^2_{Zr}\,{}^0G_{Fe:Zr} + y^1_{Zr}y^2_{Fe}\,{}^0G_{Zr:Fe} + y^1_{Zr}y^2_{Zr}\,{}^0G_{Zr:Zr} \quad (7)$$

where y_i^s is the site fraction of *i* on the sublattice *s*. The ${}^0G_{Fe:Zr}$ represents the Gibbs energy of formation of the stoichiometric compound Fe_2Zr and it is multiplied with the site fractions of Fe in first sublattice and Zr in the second. The parameter ${}^0G_{Zr:Fe}$ represents the Gibbs energy of formation of the compound Zr_2Fe (metastable) where each constituent occupies the wrong sublattices (anti-site phase). The first and last term represents the fictitious compounds formed having the same constituent in all sublattices. The site fraction is defined by

$$y_i^s = N_i^s / N^s \quad (8)$$

where N_i^s is the number of atoms of the constituent i on the sublattices s and N^s is the total number of sites on the sublattice *s*. G_m^{id} is related to the molar configurational entropy, and represents the contribution to the molar Gibbs energy assuming random mixing in each sublattice and summing these contributions considering the number of sites as follows:

$$G_m^{id} = RT\left[2(y^1_{Fe}\ln(y^1_{Fe}) + y^1_{Zr}\ln(y^1_{Zr})) + (y^2_{Fe}\ln(y^2_{Fe}) + y^2_{Zr}\ln(y^2_{Zr}))\right] \quad (9)$$

where the superscripts denote the sublattices, not a power. Finally, the ${}^{ex}G_m$ is the excess contribution to the molar Gibbs energy due to interaction between *Fe* and *Zr* in the C15 phase, described by the regular solution parameter as in chapter 3.

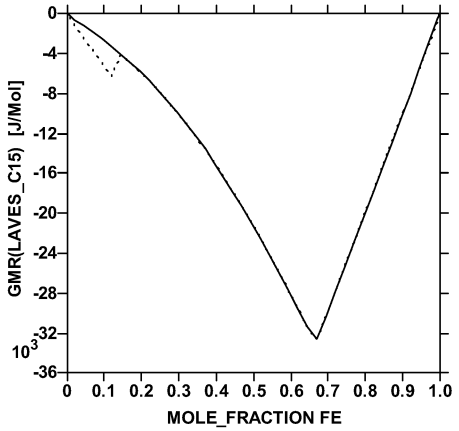

FIG 2.1 Gibbs energy of the Fe_2Zr Laves_C15 (continuous line) and the anti-site phase Zr_2Fe (Laves_C15) the dashed line. (calculated using the Fe-Zr binary system contained is the database presented in this thesis by Servant *et al*. [74]

The Gibbs energy of the C15 phase according to the model at varying Fe content is shown in Fig 2.1. The stability is maximum at the composition x(Fe)=0.67 where the Gibbs energy of the Laves_C15 has its minimum. A decrease on Fe content of this phase implies an increases on the Gibbs energy. If an external energy is input, the anti-site phase Zr_2Fe starts to appear at lower iron content. The dashed curve represents the Gibbs energy of a C15 anti-site phase. As more and more energy is input, the lattice will accommodate more and more defect until the spacial configuration of the atoms on the original C15 (long range order) is lost.

Amorphization of the secondary phase particles has been reported also in the E365 alloy and it is dependent on the temperature, irradiation doses and the alloy composition. However, irradiation has much lower detrimental effects than that observed in zircaloys-2 and 4 [8,9,30]. In the previously mentioned works on E365 alloy, it was observed that at low irradiation doses and temperatures between 330-350 °C the precipitates β-Nb and the hexagonal Laves phase $(Fe,Nb)_2Zr$ were not affected. However, both particles loose Nb and Fe respectively, and at lower temperature amophization occurs when the irradiation dose increases. The depletion of iron in the Laves particle results in an increase of the Fe content in the matrix. It was suggested that the Fe departure from the SPP causes a transformation of the Laves phase and promote the formation of the thermodynamic stable β-Nb. In the case of the $Fe(Nb,Zr)_2$ irradiation damage was not observed, however the particles tend to be coarsed [8].

2.2 Irradiation Growth

The growth due to irradiation induce a deformation of the Zircaloys and is a matter of significant technological interest. It results in a distortion of the fuel assemblies and other structural components of the core, and consists of an elongation of the Zircaloy tube. In all Zr alloys the neutron irradiation induces dislocation loops of both interstitial and vacancy characters, during irradiation they change and evolve developing a network structure. Their density mainly dependent on the irradiation temperatures and micro-structural characteristic like existence of dislocations prior to irradiation, grain boundaries [16]. In Zircaloy-2 and and Zircaloy-4 dislocation loops of <a> and <c> type are found. The irradiation produces <a> type dislocations loops, as the irradiation causes higher damage, an accelerated growth is observed, in connection to the appearance of the <c> type loops [44]. The <c> component dislocation loops are those with the Burger's vector in the [0001] direction i.e. the basal pole, these kinds of dislocations are observed to be of vacancy type and nucleated in a region adjacent to the intermetallic particles $(Cr,Fe)_2Zr$ [16, 34, 44]

The supersaturation of interstitial solute atoms or cluster of atoms in the matrix due to irradiation and the differences in their mobility, mainly between Fe and Cr [33] may enhance the Zr self diffusion [35] and probably contribute to nucleation of the dislocation <c> type loops by solute defects interaction.

In the E365 type alloy the irradiation growth is lower. This materials shows lower susceptibility to <c> evolution [8] and according to [8,9] the key factor that promote the delay in the accelerated irradiation growth in the Nb containing multicomponent Zr alloys are the composition of Nb, Fe and Sn in solid solution and the Fe/Nb ratio.

2.3 Hydrogen embritlement

The solubility of H in zirconium and its alloys is low, see in Fig 2.2. The solubility of H increases with increasing temperature. In an enlarged Zr-rich portion of the phase diagram, Fig 2.3 it is shown that at 500 °C Zr is able to dissolve up to 463 ppm H (calculated) and at 300 °C the solubility decreases rapidly to 55 ppm H (calculated). However hydrogen levels in Zr-alloys are very strict, according to the ASTM specification the alloy contains ~10 ppm H. This is due to the fact that, inside the reactor, the aqueous medium promote the formation of oxidising species, and H from the corrosion process can diffuse into the matrix material, subsequently when the solid solubility limit is reached, the precipitation of a brittle hydride occurs, see Fig 2.3. zirconium hydrides are known to precipitate as plates or as elongated groups of platelets.

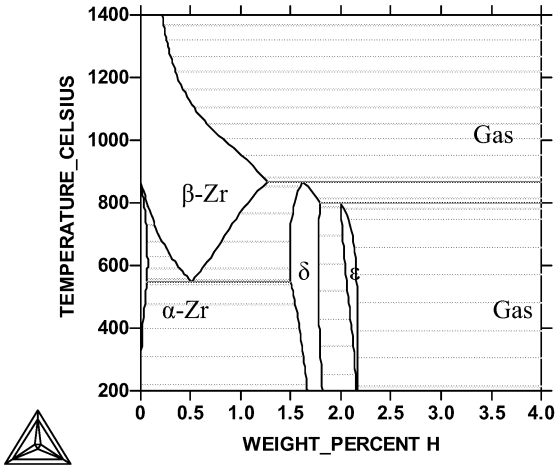

FIG 2.2 H-Zr phase diagram Dupin *et al* . [90]

The presence of a hydride has an embrittling effect on the Zr alloys due to their different properties compared with Zr alloy. On the other hand the volume fraction of the precipitated hydrides, their orientation and morphology has a pronounced impact on the severity of the embrittlement, in particular the fuel cladding. Two orientations of hydride are found in the zirconium alloys tubes: circumferential and radial.

The hydride orientation can be affected by the following factors: firstly, the crystallography, since the preference for certain plains has been observed, for example plate shape hydride was observed to precipitate on $\{10\bar{1}7\}$ [36] in zircaloy 2. Secondly, the hydrides tend to orientate parallel to the direction of rolling (the longitudinal direction of the tube) in annealed material. Thirdly, under stress the hydrides tend to align perpendicular to the tensile stress axis. Since the circumferential direction is the principal stress direction during operating conditions, for example during fuel-cladding interaction, radial oriented hydrides may serve as path for crack propagation. Hence radial hydrides

are detrimental. In order to minimize the reorientation of the hydride under stress, during the final stage of the fuel rods manufacturing process, the desired strain orientation is controlled by applying a large amount of compressive stress in the radial direction.

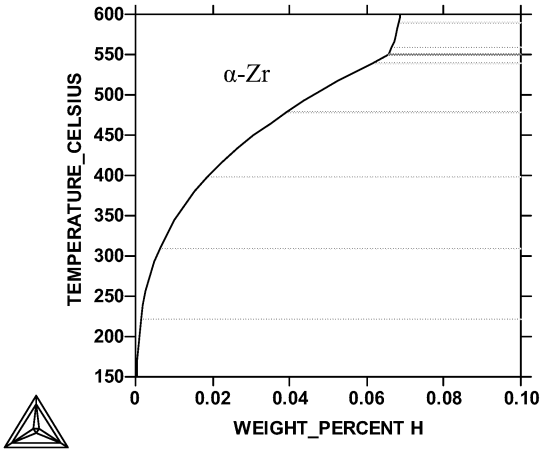

FIG 2.3 Zr rich region of the H-Zr phase diagram Dupin *et al* [90]

2.4 Corrosion (general aspects)

Corrosion and hydrogen ingress in zirconium alloys are considered directly related to in each other, due to the fact that as a result of the oxidation of the rods the hydrogen can ingress into the matrix material.

In contact with the aqueous environment, Zr alloys develop a protective dense oxide film ZrO_2 (tetragonal oxide) which later transforms into a porous oxide (monoclinic form). Microstructural changes in the ZrO_2 are believed to be an important factor to determine the corrosion resistance of the material. The microstructural changes of zirconia have been observed often to occur at the surroundings of the SPP [31] in Zircaloy 4. The oxidation of the alloying elements Fe and Cr, their incorporation into the oxide film and their tendency to dissolution will determine the corrosion resistance. According to [31,32] the SPP are incorporated into the oxide film then oxidised gradually. The oxidation of the SPP results in a volume expansion according to the Pilling-Bedworth ratio [45] producing a high local stress in the oxide. This will induce a transformation on the oxide film to balance the compressive stress created in the substrate.

The corrosion resistance of the Zircaloy-4 and Zircaloy-2 used in BWR and PWR has been found to be effected by the alloying elements: Fe, Cr, Ni (with the formation of intermetallic phases SPP) and annealing conditions in the fabrication process. Moreover the size number density and composition of the second-phase particles has a great impact in corrosion [37-41]. In the β-Zr domain, these particles are in

solution, and a treatment in the β region and quenching serves to control the size of the SPP.

During the manufacturing process a standard parameter has been commonly used for evaluation of the corrosion resistance and microstrucutre, called accumulated annealing parameter ΣA_i eq. (10), The ΣA_i parameter links the influence of the SSPs size to corrosion resistance.

$$\sum A_i = \sum t_i . e^{(-Q/RT_i)} \tag{10}$$

where
ΣA_i represents and index of the total amount of heat received during annealing in the α-phase region after the last β or (α+β) quenching.
T_i= annealing temperature in *i* Process, K
T_i=annealing time in $_i$ Process, h
Q/R= is the activation energy taken as 40000 K

According to this, the microstructure and the SPP distribution will be affected by the heat input at the processing route. In the work by Charquet [43] it was pointed out the that the reduction of the cumulative annealing parameter ΣA (conserving Fe/Cr constant) have beneficial effects on the corrosion resistance at 500 °C in steam and the important metallurgical factor is the number of precipitates per unit rather their size.

In general, the corrosion of the Zircaloys depending on the environment has different characters. For instance in boiling water reactor steam is generated inside the reactor, while in the PWR the steam is generated outside of the reactor due to the high in-reactor pressure. The BWR operates at about 290° C and 7 MPa while the PWR at about 300°C and 15 MPa. This causes dissimilar corrosion in the two reactor systems due to different water chemistry. In the boiling reactor water decomposes due to radiation, known as radiolityc decomposition, this results in production of H_2 and O_2. Consequently, an increase of oxygen in the liquid phase and hydrogen in the gas phase, in comparison to the PWR. In pressurized systems hydrogen additions between 2-4 ppm suppresses the free oxygen to very low levels ~1 ppb. In boiling water reactors the Zircaloy-2 and 4 suffer a localise surface corrosion attack, known as nodular while in PWR the surface attack has a uniform character.

The nodular corrosion occurring in BWRs (oxygenated environments) is characterized by the formation of white spots, which appears in metallographic cross sections as lense-shaped oxide. In BWRs such corrosion has been shown to depend on the coolant chemistry (water) and cladding conditions. The latter is related to the fabrication route that had been followed for a specific set of cladding. It has been generally observed that in PWR a large number of very fine SPP precipitated distribute uniformly in the matrix degrade the uniform corrosion of the Zircaloy-4 while in BWR small particle are harmless. The optimum corrosion resistance of the Nb containing multicomponent Zr alloy has been reported dependent of a uniform distribution of fine SPP (β-Nb and Fe-Nb-Zr particles) and controlled levels of Sn [42].

The composition of the matrix with O and Sn in solution have an effect on the corrosion behaviour also. The development of Zirlo see for axample [2] has shown that the corrosion resistance of zirconium alloys can be improved by decreasing the Sn

content. However a decrease in Sn has negative effects on the strengthening [45], but this has been compensated by adding oxygen.

Due to Zr high affinity to oxygen phase equilibria on the the O-Zr binary system is important. In solid solution oxygen dissolves in α-Zr phase (hcp) and in β-Zr. In the hcp lattices the oxygen atoms occupy the octahedral interstitial sites. At high temperatures, the oxygen distribution in the octahedral interstices of the sublattices defines the disorder hcp or α-Zr. The maximum solubility of O in α-Zr is 32 at. % and occurs at the eutectic T=2357 K. This solution is stable up to its congruent melting point at 29 at % O and 2400 K. At low temperature there is a transition from the disorder hcp to several ordered structures, the ordered phases are obtain by stacking a series of O atom layer parallel to the hcp basal plan in the octahedral interstices. It has been reported that below 1270 K the ordered hcp, α'-Zr is formed by a second order transformation. Other ordered hcp has been reported but in the Zr-O assessment by [91], the ordered α'-Zr has been modelled only. The order-disorder transition line α-Zr→α'-Zr is represented by the dashed line in the phase diagram, see Fig 2.4.

The compound ZrO_2 has three stable modifications: the low temperature stoichiometric compound α-ZrO_2 with monoclinic structure stable up to 1478 K, the tetragonal structure β-ZrO_2 is stable up to 2625 K and the non-stoichiometric γ-ZrO_2, which has a cubic structure (CaF_2 prototype), and melts congruent at 2995 K.

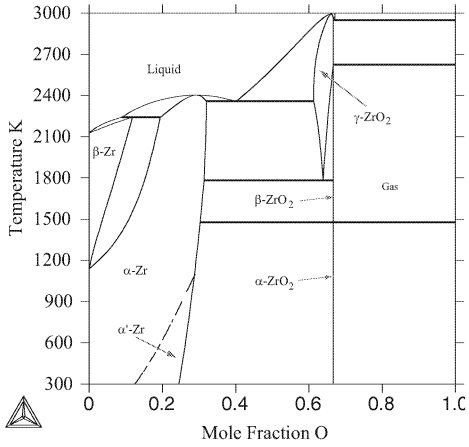

FIG 2.4 O-Zr phase diagram by Liang *et al.* [91]

2.5 Pellet-cladding Interaction

This represents a serieous problem that may lead to cladding breakdown, on one hand the fuel UO_2 deforms adopting a hour-glass form due to radial thermal gradient . In addition to these facts corrosion may also take place, caused by release of the aggressive nuclear fission product i.e. the iodine. As the fuel deforms a stress is induced on the radial direction of the claddings wall together with the cladding creep down reducing the gap between the fuel pellet and the cladding interaction results in a failure known as stress corrosion cracking SSC. In order to reduce this problem some years ago a barrier

cladding was developed which consists of an inner zirconium thin layer on the surface of the zircaloy-2 tube.

Chapter 3

Thermodynamic Database in alloy design

Computer aided phase diagram calculations based on mathematical descriptions of thermodynamic functions have became a powerful tool to predict phase behaviour in multicomponent alloys. This is the well known technique called CALPHAD (CALculation of PHAse Diagram) [46,47]. The Calphad technique has shown that reliable phase equilibria can be calculated for multicomponent alloys using assessed databases, see for example application in Al alloys by Sunders [48], in steel by Frisk and Selleby [49] and Ni alloys [50].

The energetic state of a closed system containing a great number of particles, e.g. atoms and molecules in thermal equilibrium at fixed composition, temperature and pressure, is characterised by the thermodynamic function G, i.e. Gibbs energy. The main idea of the Calphad technique is to describe the Gibbs energy of all phases in a system as a function of temperature and composition through thermodynamics models. These models are expressed in term of mathematical functions taking into account crystallography, defects and other physical properties of the phase. Once the thermodynamic description of all the phases is known, the equilibrium state can be found by minimising the total Gibbs energy of the system.

In general, all binary and ternary systems in a database are assessed from experimental data and from these realistic calculations of thermodynamic properties of higher order systems are possible. The assessment requires a detailed information about both phase equilibria (phase diagram information) and thermochemical data. Phase diagram information can include measurements on the phase equilibria for example solidus and liquidus lines. Thermochemical data consist of enthalpies, heat capacities, activities or chemical potentials. Thermodynamic descriptions of binary and ternary systems are obtained by the computerised assessment of the available experimental data. In the assessment the same data are calculated from the thermodynamic models and the difference is minimized, by varying model parameters. This step is very complex but important since the models are used to make extrapolations to higher order systems. Such calculations can be for example, the amount of stables phases, their compositions and the activity of the components.

What concerns applications for industrial alloys design at manufacturing and working temperatures, is not only the equilibrium phases but also non-equilibrium phases

that are important. The thermodynamic database also provides the possibility to extrapolate outside the stable range provided that such experimental information is available, because the modelling is done for the entire system.

In general, the models for the solid phases are based on the Compound energy formalism CEF [50]. The fundamental basis of the CEF makes use of the crystallographic information of a phase, although in some cases simplification of the structure is necessary.

3.1 The Zr Database

A database represents a collection of thermodynamic model parameters which are able to reproduce a large amount of experimental information by a small number of parameters. The basic information in the database is the unary data, i.e. the thermodynamic description of the pure elements. Those are already evaluated and compiled by the Scientific Group Thermodata Europe (SGTE). SGTE compilations are available in Therm_Calc [52] database library and can also be found in Ref. [53].

In the Zr database, the information concerning binary systems consists, partially of a collection of assessments from different sources published or unpublished. The following system were assessed in this work: Cr-Sn (paper I), Mo-Zr (paper II), Sn-Zr (paper VI) and two ternary systems Fe-Nb-Zr (paper IV) and O-Nb-Zr (paper V, extrapolated from the binaries).

The elements included in the zirconium database are: C, Cr, Fe, Mo, Nb, Ni, O, Si, Sn. The large amount of elements gave rise to 45 binary systems. This combined with the lack of experimental information in the ternary systems of the type Zr-M-M, where M represent any alloying elements, complicated the database creation task. Thus some simplifications where made taking into account priority systems. For the binary case it was decided to include the description of all the binary systems of the type Zr-M (M= C, Cr, Fe, Mo, Nb, Ni, O, Si, Sn. Systems of the type M-M were included either because they will be necessary to describe the ternary systems or for the relevance of the case, for example Sn-Nb, Fe-Nb, Mo-Zr. The binary Zr-H was added, due to the importance of the hydrogen embritlement. For the ternary case, the list of systems became much larger than the binary list. The lack of experimental information related to ternary systems made the assessment task impossible without new experimental information. Priority criteria was used to choose significant ternary systems. Thus, considering the fact that zirconium alloys interact strongly with oxygen both during manufacturing of the alloys and *in-reactor* performance, the O-Sn-Z is considered very important for Zircaloy-2 and Zircaloy-4 and for the same reason the Nb-O-Zr in Nb containing multicomponent alloys: Zirlo, and E635. The phase equilibria in the ternary Fe-Nb-Zr makes a very good representation of the relative new generation of zirconium alloys: Zirlo and E635. The intermetallic compounds present in this ternary system are important precipitates in those alloys, see chapter 1. For the same reason the phase equilibria in the Zr-Fe-Cr and Zr-Fe-Ni are also important in Zircaloy-2 and Zircaloy-4.

3.2 Thermodynamic Modelling

3.2.1 Pure Elements

The Gibbs energy, ${}^{0}G$, of the pure constituents i at temperature and physical state of interest is given relative to the enthalpy of the element in its stable state at 298.15

K and the entropy at 0 K. It is expressed using the power series in T shown in eq.(11) SGTE [53] has evaluated the Gibbs energy expression of pure elements in all stable and many meta-stable states for the temperature range 293-6000 K.

$$ {}^{0}G_i - H_i^{SER} = a + bT + cT\ln T + \sum_n d_n T^n \tag{11} $$

where $n = 2, 3, -1\ldots$

3.2.2 Solution phases

The thermodynamic models for the Gibbs energy of a phase can be represented by the general eq.(12)

$$ G_m^{\phi} = {}^{ref}G_m^{\phi} + {}^{id}G_m^{\phi} + {}^{ex}G_m^{\phi} + {}^{mag}G_m \tag{12} $$

In metallic systems, solution phases (liquid, bcc, bct, fcc, hcp) are modelled assuming random mixing of the atoms. For each phase the molar Gibbs energy of formation is expressed by the eq. (12)

$$ G_m^{\phi} = \sum x_i^{\phi} G_i^{\phi} + RT\sum x_i^{\phi}\ln x_i^{\phi} + {}^{ex}G^{\phi} + {}^{mag}G \tag{13} $$

In the first term, ${}^{0}G_i^{\phi}$, represents the Gibbs energy for the pure element *i* in the phase ϕ (liquid, bcc, hcp..), always given relative to the pure element reference state SER. The second term, $RT\sum x_i^{\phi}\ln x_i^{\phi}$ represents the contribution due to random mixing of the atoms and x_i is the mole fraction of the component. The third term, ${}^{ex}G_m^{\phi}$, is the excess Gibbs energy. It represents the deviation from the ideal behaviour. For a multicomponent system the excess term contains binary, ternary and higher order interactions. A general formula for the binary contribution is given by the sum over all interactions:

$$ {}^{ex}G_m = \sum_{i=1}^{n-1}\sum_{j=i+1}^{n}\left(x_i x_j\right)L_{ij} \tag{14} $$

For the ternary contribution, the excess ternary interactions in the eq (14) turns to:

$$ {}^{ex}G_m = \sum_{i=1}^{n-2}\sum_{j=i+1}^{n-1}\sum_{k=j+1}^{n-1}\left(x_i x_j x_k\right)L_{ijk} \tag{15} $$

and each binary L_{ij} term can be expanded by Redlich-Kister polynomial:

$$ L_{ij} = \sum_{i\neq j} x_i x_j \left\{{}^{0}L + (x_i - x_j)^{1}L + (x_i - x_j)^{2}L\ldots\right\} \tag{16} $$

the L_{ij} can be linearly temperature dependent, the temperature dependence of the parameter is represented as:

$$^{n}L_{i,j} = A + BT \tag{17}$$

For a binary, the excess Gibbs energy takes into account the chemical interaction between the constituents *i* and *j* (L_{ij}) in the ϕ phase The coefficients $^{n}L_{ij}^{\phi}$ are obtained from the least-square optimisation fitting of experimental data. In the eq. (16) when *n*=0, it corresponds to the regular model. When *n* takes values 1 and 2 the model is called sub-regular and sub-sub regular model respectively. It is desirable to evaluate as few parameters as possible in order to keep the physical meaning of the modelling and to have more realistic extrapolations of the phases.

The fourth term in eq. (18), ^{mag}G represents the magnetic contribution to the Gibbs energy for elements which displays magnetic ordering. This contribution is treated with an additional empirical formula according to the model by Hillert and Jarl [54] and Inden [55]. Thus for pure elements and solutions phases the magnetic contribution is given by:

$$^{mag}G = RT\ln(\beta+1)f(\tau) \tag{18}$$

where, τ=T/T* and T* the critical temperature for magnetic ordering in ferromagnetism known as T_c (Curie Temperature) for anti-ferromagnetism as T_N (Neel temperature), β denotes the average magnetic moment per atom given in unit of Bohr magnetons. The function $f(\tau)$ for different phases is given in Ref. [55]. The composition dependence of T_c or T_n and β in alloys is described in the same way as the excess Gibbs energy

3.2.3 Stoichiometric Compounds

The Gibbs energy of a stoichiometric compound φ at temperature T is given as the Gibbs energy of the compound φ relative to the pure constituents in their stable state of reference and multiplied by the stoichiometric coefficient a_i of the constituents *i.*

$$^{0}G^{\varphi} - \sum a_i\,^{0}H_i^{SER} = A + BT + CT\ln T + ... \tag{19}$$

Usually during the optimization the first two term are evaluated. Additional terms are possible to evaluated if thermo-chemical data is available, i.e. Cp. Otherwise the Neumanm- Kopp rule [103] can be used for the Cp, extrapolating this property from the pure elements.

3.2.4 Compound Energy Formalism CEF

The CEF also called the sublattice model, was introduced by Hillert and Staffansson [49], and later extended by Sundman and Ågren [50].

CEF basically defines different crystallographic sites i.e. sublattices in which various constituents can mix. Hence, in CEF the molar Gibbs energy of a phase is determined by the site occupation of the constituents in different sublattices This fractional site occupation is known as site fraction and it is defined by eq. (20):

$$y_i^s = N_i^s / N^s \tag{20}$$

where, N_i^s is the number of atoms of the constituent i on the sublattices s and N^s is the total number of sites on the sublattice.

This formalism is employed to describe solution phases like hcp, bcc or fcc with interstitially dissolved atoms, like O, C or H mixed with vacancies and for intermetallic compounds that show composition variation.

Many intermetallic phases do not have a fixed composition but they appear in a composition range. In general, this can be explained by the fact that crystals are not perfect and defects can occur in the lattice structure. In this particular case point defects, vacancies and anti-site atoms (substitutional or interstials atoms) are the interesting ones. When developing the models, the crystallographic information of the phase is important, for example, site occupancy of the atoms can provide a guide for the choice of sublattice model.

When modelling a compound A_aB_b in a binary system with anti-site atoms on both sublattices, the sublattice model is represented as follows:

$$(A,B)_a(A,B)_b$$

The Gibbs energy of this phase is also expressed by the eq. (14), Thus, having only one constituent in each sublattice defines a compound and reference surface for the Gibbs energy is obtained by random combination of all such compounds.

$${}^{ref}G_m = y_A^1 y_A^{2\,0}G_{A:A} + y_A^1 y_B^{2\,0}G_{A:B} + y_B^1 y_A^{2\,0}G_{B:A} + y_B^1 y_B^{2\,0}G_{B:B} \tag{21}$$

where, the subscript represent the sublattice, not the power.

It is assumed that the constituents i and j mix randomly on each sublattice and the total entropy of mixing depends on the number of sites, a and b. Thus, the ideal entropy contribution to the Gibbs energy is expressed as follows:

$$G_m^{id} = RT\left[a(y_A^1 \ln(y_A^1) + y_B^1 \ln(y_B^1)) + b(y_A^2 \ln(y_A^2) + y_B^2 \ln(y_B^2))\right] \tag{22}$$

The excess contribution to the molar Gibbs energy ${}^{ex}G_m$ is described by the interaction between at least two constituents in the same sublattice, in this way the substitutional or interstitial defects are considered. Vacancies can also be taken into account if such a defect is supported by experiments.

$${}^{ex}G_m = y_A^1 y_B^1\left(y_A^2 L_{A,B:A} + y_B^2 L_{A,B:B}\right) + y_A^2 y_B^2\left(y_A^1 L_{A:A,B} + y_B^1 L_{B:A,B}\right) \tag{23}$$

This method to model phases with composition variation becomes more complex when a component is added i.e. a ternary system. If two such binary phases, like $(A,B)_a(A,B)_b$ and $(A,C)_a(A,C)_b$, dissolve each other the model becomes

$$(A,B,C)_a(A,B,C)_b.$$

$$^{ref}G_m = y_A^1 y_A^2\,{}^0G_{AA} + y_A^1 y_B\,{}^0G_{AB} + y_A^1 y_C^2\,{}^0G_{AC} + y_B^1 y_A^2\,{}^0G_{BA} + y_B^1 y_B^2\,{}^0G_{BB} + y_B^1 y_C^2\,{}^0G_{BC} + y_C^1 y_A^2\,{}^0G_{CA} + y_C^1 y_B^2\,{}^0G_{CB} + y_C^1 y_C^2\,{}^0G_{CC} \quad (24)$$

In this case parameters like $^0G_{BC}$ are needed, representing a compound on the B-C binary which may not be stable.

3.2.5 The ionic model (liquid phase)

When dealing with oxide systems a special variant of the sublattice model is used to describe the liquid phase.

In the Zr-base database, the substitutional model used to describe the liquid in some of the original assessed binaries has been replaced by the two sublattice model for ionic liquid. This was done in order to make the models that describe the metal-metal and metal-oxygen systems compatible. Those two models are identical for binary systems [56] hence no reassessment is required.

In the two sublattices model for the ionic-liquid, cations (C) with valence V_C occupy the first sublattice and anions (A) with valence V_A, hypothetical vacancies (Va) and/or neutral species (η) occupy the second sublattice as follows:

$$(C^{V_C})_P\,(A^{V_A}, Va, \eta)_Q$$

This model can describe the liquid from the pure liquid metal to the liquid oxide in equilibrium with the oxygen gas. Since the sublattices are occupied by charged species and the electroneutrality in the phase must be kept, the stoichiometric coefficients P and Q vary with composition [85Hil]. P and Q represent the average charge in each sublattice and V_{va} an " induced " charge in the vacancies:

$$Q = \sum V_c y_c = -V_{Va} \quad (25)$$

$$P = -\sum V_A y_A + Q y_{Va} \quad (26)$$

3.3 The assessments

The assessments were performed using the optimisation module Parrot of Thermo-Calc. In this module experimental data on phase equilibria and thermo-chemical properties are optimised simultaneously by means of a least square method.

During the optimisation the CALPHAD technique is employed. It is summarised in the following steps:

1. Selection of a suitable model for each phase.
2. Critical analysis of the available experimental data.

3. Computerised evaluation of the experimental data in terms of model parameters.

In step one, an appropriate model is chosen in order to describe the individual properties of each phase. This step is very important because the thermodynamic properties of a higher order system are extrapolated from the binary and the accuracy of these extrapolations depends strongly on the selected model.

In the second step the experimental data are analysed and inconsistent set of measured values are excluded from the optimisation. A reasonable procedure to do that is to carefully go through the experimental techniques used for the measurements to find possible sources of error. Especially, for reactive materials like in our case Zr, problems due to impurities and oxidation may lead to complications in the experimental data. Reactions with crucible are also of concern. Sometimes the sources of error are not obvious, this problem can be tackled by direct calculations. This means that all available experimental data is used in the beginning of the optimisation. If a set of conflicting data can be identified by the fact that it is more difficult to fit than all the rest. It may then be rejected for the final optimisation. Preferably, both phase diagram information and thermochemical data are used. Phase diagram information can include measurements of phase equilibria for example solidus and liquidus lines. Thermochemical data include enthalpies, activities or chemical potentials. However, this experimental information is not always available. It is therefore of great help to make use of quantum mechanics which allows to calculate properties of well defined materials with high levels of accuracy. In particular the information one wishes to extract from these calculations is the total energy for different arrangement of atoms on different lattices for pure elements and compounds and from this the enthalpy of formation of the compounds of interest.

In the second and third step which often has to be iterated several times, the calculations from the thermodynamic models are compared with the experimental information using the least square method. Final values for the model parameters are obtained by minimising the statistical error between calculated and measured values, considering the uncertainty for each experiment.[57]

The least square optimisation make use of the best fit criterion which is derived from the maximum likelihood principal. It states that "*the set of available experimental observation should appear to be the most likely when taken as a whole*"[58]. In the least square method it is assumed that the experimental errors are random and uncorrelated and the distribution of measured values about their true value follows the normal Gaussian distribution.

The files with the binary systems are merged in a single file using MERGER software [59]. This program has been developed for the construction of databases with Thermo-Calc structure.

3.4 Contributions to phase diagram calculations: Quantum mechanic and Miedema´s semiempirical macroscopic model.

The lack of thermodynamic information like enthalpy of formation of intermetallic compounds is a problem of big concern for the assessor of binary or ternary phase diagram. Many have solved these problems by replacing the lacking data using either Miedema´s model [62] estimated values or the *ab initio* calculated values [104]. For instance in several alloys systems thermodynamic properties have been described by combining quantum mechanical calculations (*ab-initio*) and CALPHAD method

[5,60,61]**.** Both Miedema estimated values and *ab initio* calculation offer valuable help when experimental information is missing and when dealing with experimental difficulties, for example, if reactive materials are involved. However there exists a substantial difference between these two methods. The *ab initio* method makes use of quantum mechanical electronic band calculation to describe the chemical bonding of the elements in consideration. This implies solving the Schrödinger equation for electronic wave-functions in the unit cell. In order to perform such calculations, specific information is needed on the atomic numbers of the constituents and on their arrangement in space (atomic positions and translation vectors in the unit cell of the structure). Then lattices structures which possess the lowest total energy are obtained. The minimization of the total energy is found with respect to volume (volume relaxation), the unit cell (for internal relaxation) and the position of the atoms within the cell (cell internal relaxation) for the atoms which has deviated from their positions (high-symmetry imposed by the space group). These calculations are done for pure elements and compounds in solid state at 0 K.

The enthalpy of formation, $\Delta_f H$, is extracted from the total energy minimum by subtracting the concentration weighted total energy minimum of pure element.

$$\Delta H^{form}_{A_{1-x}B_x} = H^{\min}_{A_{1-x}B_x} - (1-x)H^{\min}_{A} - xH^{\min}_{B} \tag{27}$$

Miedama's method represents a parametrized atom model which systematizes the data base available for alloys formation [62,63,64]. In this model it is assumed that the atoms have the same macroscopic properties as the corresponding elements. Hence electronic properties like density and chemical potential for electron are estimated from the ratio bulk modulus K and molar volume V_m and enthalpies are derived from them. In the Miedema´s method the structure-dependent contributions to phase stability is not considered. Despite this fact in certain cases Miedema's model is capable of predicting enthalpy of formation with relatively good accuracy compared to experimental values, see for example Refs. [63,65].

On the other hand, it is also important to point out that in *ab initio* calculations the electronic-ion interactions are described by different methods and the potential obtained for this interactions are either truncated (Pseudopotential method) or not (Full potential method). The advantage of the Pseudopotential method in relation to the full potential methods is the decrease in computing time but the degree of accuracy is decreased too. Nevertheless the increasing computer power through the years has contributed to achieve more reliable results.

Chapter 4

Description of the Zr Database and its further development

The basis for a thermodynamic database for zirconium alloys has been developed. This project was carried out at the Department of Materials Science and Engineering in KTH under the supervision of Prof. Bo Sundman at the division of computational thermodynamics. The work was sponsored by the Swedish Nuclear Power Industry: OKG Aktiebolag, Forsmarks Kraftgrupp AB Ringhalsverket, SKI, Barsebäck Kraft AB and Westinghouse Electric Sweden.

The aim with this work is to reduce the amount of experimental work necessary under the manufacturing process for the design of new alloy composition by using thermodynamics to perform equilibrium calculations in multicomponent and multiphase systems.

The purpose of this chapter is to provide a guide for future users of this database as well as to provide facilities for its further development. The present database constitutes a combined work which includes thermodynamic assessment from various sources and performed assessment.

4.1 Zirconium alloys database content

Is a database for fuel cladding application and contain 9 elements:

C, Cr, Fe, Mo, Nb, Ni, O, Si, Sn, Zr + H

It includes the following assessed system: C-Zr [66], Cr-Sn [67], Cr-Fe [68,92], Cr-Nb [69], Cr-Ni [70,93], Cr-Zr [71], Fe-Nb [72], Fe-Ni [70,29], Fe-Sn [73], Fe-Zr [74], Ni-Sn [75], Ni-Zr [76, zircobase] Mo-Zr [77], Mo-Ni [78], Mo-Si [79], Nb-Sn [80], Nb-Zr [81], Si-Zr [82], Sn-Zr [83], Fe-Nb-Zr [84], Cr-Ni-Zr [85], the assessed oxide systems: Cr-O [86,29] , Ni-O [86,94], Cr-Ni-O [86], Cr-Fe-O [87], Fe-O [88,94], Fe-Ni-O [89], O-Sn [90], O-Nb [90], O-Nb-Zr [8], O-Zr [91] and H-Zr [90].

[8] The O-Nb-Zr is extrapolated from the binaries

In the database the Gibbs energy of all the components and all phases of the system are described as functions of temperature and composition. With this thermodynamic description the equilibrium state is calculated by minimizing the total Gibbs energy of the system.

4.2 Method

The main technique is to use experimental information on phase diagram and thermo-chemistry and analyse it using mathematical models which describe the properties of the phases, this is also referred to as the Calphad technique. Consistent models must be used for the pure elements and for the phases (binary ternary or higher order) in order to combine results from independent assessments in a common database. Those models are able to describe a large amount of experimental information by small amount of model parameters.

4.3 Description and recommendations

In Table 1 all phases present in the database are listed. For some of the intermetallic phases the corresponding prototype structure is given. In some systems a miscibility gap can occur, in that case the system is given in a footnote.

4.3.1 The hcp phase

Some adjustments were done in the hcp phase in order two merge the files with metal-metal (M-M) where the model is $(M)_1\ (Va)_{0.5}$, (M= Cr, Fe, Ni, Nb, Mo, Si, Sn and Zr) systems and H-Zr and O-Zr where the models are $(Zr)_1\ (Va)_1(H)_1$ and $(Zr)_1\ (O,Va)_1(Va,)_1$ respectively.

In the model the second sublattice represents the octahedral interstitial occupied by O and Va and the third represents the interstitial occupied by hydrogen. Note that the C-Zr system is included in the database but the model is not compatible for hcp. In order to avoid problems in the calculations when having both C and O , this problem must be corrected. In the database the hcp is modeled as follows:

$$(M)_1\ (C,O,Va)_1(H,Va)_1$$

4.3.2 The liquid phase

In the Zr-base database, the substitutional model used to describe the liquid in some of the original assessed binaries has been replaced by the two sublattice model for ionic liquid. This was done in order to make the models that describe the metal-metal and metal-oxygen systems compatible. These two models are identical for binary systems. In the two sublattices model for the ionic-liquid, cations (C) with valence V_C occupied the first sublattice and anions (A) with valence V_A, vacancies (Va) and/or neutral species (η) occupy the second sublattice as follows:

$$(C^{V_C})_P\ (A^{V_A}, Va, \eta)_Q$$

The stoichiometric coefficients P and Q vary with composition P and Q represent the average charge in each sublattice.

4.4 Database extensions

In the appendix of this thesis is provided a list of older references on phase equilibria information for some ternary systems of the type M-M-Zr and M-O-Zr. In key systems like Cr-Fe-Zr, Fe-Ni-Zr, Fe-Nb-Zr, O-Sn-Zr the experimental information is very scarce.

The Cr-Ni-Zr ternary system has been extracted from the assessment published in Ref. [85]. This assessment is based on the experimental work on the Laves phase domain extension across the ternary composition triangle at 1273 K publish in ref [95]. The Zr rich corner is extrapolated from the binaries, and in order to verify the accuracy of the extrapolations, new experiments are desirable.

The Fe-Nb-Zr system is a preliminary assessment performed at 1073 K, which can be improved with more experiments. Fe-Zr binary has to be reassessed, according to the experiments by Stain *et al*. in [96], the Laves_C36 is stable in this binary, $FeZr_2$_C16 is a high temperature phase stable between 1048-1247 K, and the $Fe_{23}Zr_6$ is not an equilibrium phase in this system. Nevertheless, a new assessment of this binary system will soon be available [97].

The O-Nb-Zr ternary system included in this database consist of extrapolations from the binary system. The accuracy of the extrapolations have been tested and compared with the experimental data on the ternary system, see paper V in this thesis. In Appendix 1, references on O-Nb-Zr experimental data are given.

The secondary phase particle SPP, present in Zr alloys: $(Fe,Ni)Zr_2$_C16 (tetragonal C16) and $(Cr,Fe)_2Zr$ (Laves C14 or C15) in Zircaloy-2 and Zircaloy-4 and $Fe_2(Zr,Nb)$ Laves_c14 and $Fe(Zr,Nb)_2$ (Cubic C16) in Zirlo and E-365, have provided a guide for selection of more important ternary systems, for example: Fe-Nb-Zr, Cr-Fe-Zr, Fe-Ni-Zr, Cr-Ni-Zr. Regarding Fe-Ni-Zr and Fe-Cr-Zr new experimental data have been published by Barberis *et al.* [5] and can be used with older data (appendix 1) for the assessment.

Due to the fact that zirconium alloys interact with oxidant environments in the manufacturing process and with H_2O during *in service* operation oxygen and hydrogen are two very important element in this database. Binary systems of the type M-O (C, Cr, Fe, Mo, Nb, Ni, Si, Sn, Zr) are essential for further study of the phase equilibria in higher order systems like Zr-M-O or M-M-O. A better understanding of the phase equilibria including oxygen are important not only for the effect of this element on the α-Zr↔β-Zr transition temperature but it can also, give valuable information on the thermodynamic stability of the phases forming after the oxidation of the SPPs.

Moreover, phase diagram calculation can be useful on modelling of severe industrial accidents. As an example the Fe-O-Zr and U-O-Zr ternary system are important for modelling the high temperature equilibria in the quaternary system Fe-O-U-Zr which represents hypothetical accidents involving core melting. The thermodynamic assessment of those systems are available in the literature. However the compatibility of the models has to be checked, specially the liquid phase, the hcp and the oxides**.**

4.4.1 The O-Sn-Zr

The experimental data in the O-Sn-Zr ternary system are limited. The zirconium rich corner has been investigated using metallographic studies, X-ray diffraction and electron probe micro- analysis (EPMA) by Aricó *et al*. [99], and Aricó and Gribaudo [100]. At 1287 K [36Ari] found a three phase equilibrium between: α-Zr(O,Sn)+Zr_5Sn_3 +αZrO_2. They found the same equilibrium at 1587 K and the equilibrium compositions were almost the same. In Fig 4.1 the phases in equilibrium at the zirconium rich corner are shown. [100] measured the phase compositions of an isothermal annealed sample at T=1287 and 1573 K and proposed a tentative boundary for the α-region. No ternary intermetallic compound was reported. According to [99] and [100] the only ternary phase is this system is the solid solution α-Zr(Sn,O).

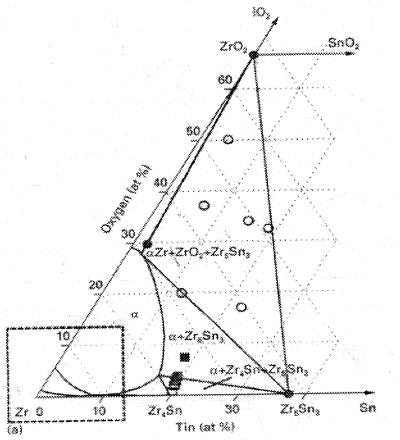

FIG 4.1 Zirconium rich corner of the O-Sn-Zr ternary system, isothermal section at 1287 K [99]

Fig. 4.2 shows in more detail the equilibria surrounding the α-Zr phase (α-Zr(Sn,O)) and the β-Zr phase (β-Zr(Sn,O)).

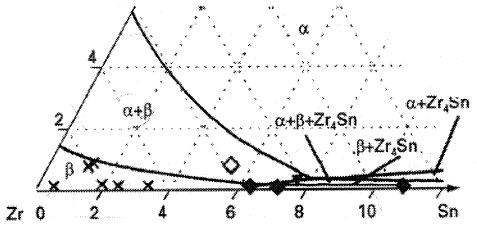

FIG. 4.2 Equilibria surrounding the α-Zr phase in O-Sn-Zr at 1287 K according to [100]

In X-ray studies [100] found some variation of the lattices parameters of the Zr_5Sn_3 and according to them it is due to the interstitial dissolution of oxygen in the

intermetallic. The proposed boundary is show in the Fig 4.3 where the solubility of Sn in α-Zr also has been drastically reduced compared to [99]. It has been mentioned that Kwon and Corbett [101] studied the influence of impurities (O, Fe etc) in Sn-Zr binary system. In these studies they contemplate a possible compound $Zr_5Sn_3O_x$ for x=0.1 and 0.5. However, [99] and [100] did not mention any dissolution of oxygen in this phase.

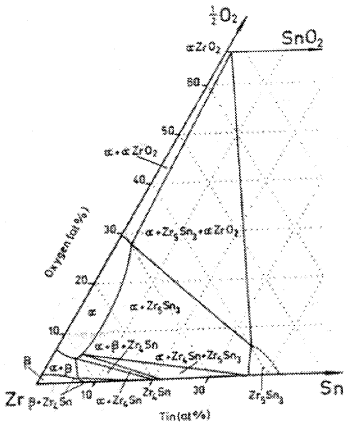

FIG. 4.3 Isothermal section at 1323 K (O-Sn-Zr) [100]

There is a large difference in the α-Zr phase field in Ref. [100] and in Ref. [101]. The reason for this is not explained in the papers, hence new experiments on the O-Sn-Zr ternary system were designed. Since those experiments are a collaboration between KTH and CEA (France), they will be soon available for an assessment of O-Sn-Zr ternary system.

Table 1 Phase present in the database

Phase	*Prototype structure*	*System*	*Comments*
Ionic-Liq	-		This phase contains: C, Cr, Fe, H, Mo Nb, Ni, O, Si, Sn, Zr Miscibility gap [9]
BCC_A2			This phase contains: C,Cr, Fe, Mo, Nb, Zr Miscibility gap [10]
BCT_A5			Sn
FCC_A1			This phase contains: C, Cr, Fe, Ni
HCP_A3			This phase contains: C, Fe, Mo, Ni, Nb, O, Si, Sn, Zr
A15	Cr_3Si (cubic)	Nb-Sn Sn-Zr	Nb_3Sn $SnZr_4$
B35	CoSn	Fe-Sn	FeSn
	NaCl	C-Zr	Carbide CZr_x

[9] Fe-Sn, O-Sn, Cr-Sn
[10] Nb-Zr, Fe-Cr

	(cubic)		(fcc_A1)
C1	CaF_2	H-Zr	H_2Zr-δ hydride
			(fcc_C1)
	ThH_2	H-Zr	H_2Zr-ε
C14	$MgZr_2$	Cr-Nb	
	(Hexagonal laves)	Cr-Zr	
		Fe-Nb	
		Fe-Zr	metastable
		Fe-Nb-Zr	$(Nb,Fe)_2Zr$
C15	Cu_2Mg	Cr-Nb	
	(Cubic Laves)	Fe-Zr	
		Mo-Zr	
	$NiTi_2$	Fe-Zr	metastable
	(Cubic)	Ni-Zr	$NiZr_2$
		Cr-Ni-Zr	$(Cr,Ni)Zr_2$
		Fe-Nb-Zr	$Fe(Nb,Zr)_2$
			Called in the database MZr_2_cub
C16	Al_2Cu	Fe-Zr	$FeZr_2$
	(Tetragonal)	Fe-Sn	$FeSn_2$
		Si-Zr	$SiZr_2$
C21	TiO_2	O-Sn	O_2Sn
			(Brookite)
C36	$MgNi_2$	Cr-Zr	Cr_2Zr
	(Hexagonal Laves)	Fe-Zr	metastable
O_2Zr	CaF_2	O-Zr	O_2Zr_cubic
	cubic		
O_2Zr	HgI_2	O-Zr	O_2Zr_tetr
	tetragonal		
O_2Zr		O-Zr	O_2Zr-monocl.
C49	Si_2Zr	Si-Zr	Si_2Zr
C54	$TiSi_2$	Sn-Zr	Sn_2Zr
$D0_{19}$	Ni_3Sn	Ni-Zr	Ni_3Zr
$D5_a$	Si_2U_3	Si-Zr	Si_2Zr_3
	Mn_5Si_3	Si-Zr	Si_3Zr_5 ?
	(Hexagonal)	Sn-Zr	Sn_3Zr_5
Ga_4Ti_5	Hexagonal	Sn-Zr	Sn_4Zr_5
E1A	BRe_3	Fe-Zr	$FeZr_3$
	(orthorhombic)		
Fe_5Sn_3		Fe-Sn	Fe_5Sn_3
Fe_3Sn_2		Fe-Sn	Fe_3Sn_2
Mo3Si		Mo-Si	Mo3Si
$MoNi_3$_gamma		Mo-Ni	$MoNi_3$_gamma
$MoNi_4$_beta		Mo-Ni	$MoNi_4$_beta

MoNi_delta		Mo-Ni	MoNi_delta
$MoSi_2$		Mo-Si	$MoSi_2$
Mo_5Si_3		Mo-Si	Mo_5Si_3
Nb_6Sn_5	Sn_5Ti_6	Nb-Sn	Nb_6Sn_5
$NbSn_2$	$CuMg_2$	Nb-Sn	$NbSn_2$
Nb_6Sn_5	Sn_5Ti_6	Nb-Sn	Nb_6Sn_5
Ni_5Zr	$AuBe_5$	Ni-Zr	Ni_5Zr
Ni_3Sn_HT		Ni-Sn	Ni_3Sn high temperature
Ni_3Sn_LT		Ni-Sn	Ni_3Sn low temperature
Ni_3Sn_LT		Ni-Sn	Ni_3Sn low temperature
Ni_3Sn_4		Ni-Sn	Ni_3Sn_4
NiZr	BCr	Ni-Zr	NiZr
SiZr		Si-Zr	SiZr
Ni_7Zr_2	Ni_7Zr_2	Ni-Zr	Ni_7Zr_2
		Cr-Ni-Zr	$(Cr,Ni)_7Zr_2$ Called in the database Ni_7Zr_2
$Ni_{10}Zr_7$	$Ni_{10}Zr_7$	Ni-Zr	$Ni_{10}Zr_7$
$Ni_{21}Zr_8$	Hf_8Ni_{21}	Ni-Zr	$Ni_{21}Zr_8$
$Ni_{11}Zr_9$	$Pt_{11}Zr_9$	Ni-Zr	$Ni_{11}Zr_9$
NbO		Nb-O	NbO
NbO_2			NbO_2
Nb_2O_5			Nb_2O_5
$SiZr_3$	PTi_3	Si-Zr	$SiZr_3$
Si_4Zr_5	Si_4Zr_5 ?	Si-Zr	Si_4Zr_5
Sigma		Fe-Cr, Fe-Cr- Ni	
Diamond_A4		Si	
Corundum		Cr-O, Cr-Ni O	
		Cr-O	Cr_30_4
Halite		Fe-O, Ni-O, FeNi-O	
Spinel		Fe-O, Ni-O, Fe-Ni-O	

The gas phase contains the following species

Species	*System*
H, H_2, HZr Zr, Zr_2	H-Zr
O2	Ni-O, Zr-O, Cr-O, Fe-O
O, O2 O3, Zr, $Zr0_2$	Zr-O
Nb,NbO,NbO_2,O,O_2,O_3	Nb-O
O,O_2,O_2Sn,O3,OSn,Sn,Sn_2	Sn-O

Chapter 5

Concluding Remarks

5.1 The papers in this work

5.1.1 Summary of paper I

Thermodynamic assessment of the Cr-Sn binary system

Rosa Jerlerud Pérez and Bo Sundman

In this paper the thermodynamic description of the Cr-Sn binary system was obtained by means of the Calphad technique. In order to compensate the lack of thermodynamic information of this system, the estimated enthalpy of mixing from Miedema was used as supplementary information. The phases in equilibrium in this system are: the solid solution phases Cr-bcc (body centered cubic) the Sn-bct (body centered tetragonal) and the liquid. The miscibility gap was difficult to reproduce and more experimental data is required in order to judge the accuracy of the assessment of this system.

5.1.2 Summary of paper II

Thermodynamic assessment of the Mo-Zr binary phase diagram

Rosa Jerlerud Pérez and Bo Sundman

In this assessment fairly good agreement is observed between the calculated phase diagram and the available experimental data (phase diagram data). Nevertheless the calculation disagrees with some of the experiments at the zirconium rich side. It is suspected that the experimental liquidus has been contaminated due to the high reactivity of zirconium. The lack of thermodynamic information (enthalpies, activities) in this system was compensated by estimated enthalpy values: the enthalpy of formation of the Laves phase and the enthalpy mixing of the liquid.

5.1.3 Summary of paper III

Structural stability of intermetallic phases in the Zr-Sn system

V.I. Baykov, Rosa Jerlerud Perez, P.A. Korzhavyi, Bo Sundman and B.Johansson

In this paper, the thermodynamic properties of the intermetallic compounds in the Zr-Sn binary system were obtained by first principle calculations of the total energy of the compound at 0 K, using the Vienna *ab initio* code VASP. The method used in VAPS is based in the local density functional (LDF) theory [104]. The calculated lattice parameters of the equilibrium phases in this system are reported, as well as the estimated formation energy of these compounds by means of Miedema´s method. All theses quantities are compared with the available experimental data.

In the theoretical study presented in this paper, two problems were treated: the thermodynamic stability of Zr_5Sn_4 compound in this system and the determination of the type of structural defects in the Zr_4Sn compound which cause the deviation from the ideal stoichiometry suggested by its structure A15 (Cr_3Si prototype). Two possible structures derived from A15 were studied :vacancies on the Sn sublattice $Zr_3(Sn_{.75}\ Va_{.25})$ and Zr substitution on the Sn sublattice $Zr_3\ (Sn_{.8}\ Zr_{.2})$.

The Zr_5Sn_4 compound was found to be a stable phase in this system. The Zr_5Sn_3 Zr_5Sn_4 compounds both with a hexagonal lattice shown the most negative energies. The results of the calculations of the density of state (DOS) for both compounds revealed that, the hybridisation of the Sn 5*p* with Zr 4*d* electronic states is the reason of their high stability.

In the case of the Zr_4Sn phase, for the vacancy model, it was calculated the formation energy of the $Zr_3(Sn_{0.75},Va_{0.25})$ compound using a supercell with 64 sites, i.e. $Zr_{48}(Sn_{12}Va_4)$, arranging the four vacancies in the structure of the supercell of the fcc lattice. For the Zr substitution on the Sn sites was considered 4 model alloys, described by supercells of various size, $Zr_{48}(Sn_{15}Zr_1)$, $Zr_{48}(Sn_{13}Zr_3)$, and $Zr_{48}(Sn_{12}Zr_4)$. The alloy with the configuration $Zr_{48}(Sn_{13}Zr_3)$ was found to be the most stable and has the stoichiometry (79.687 at % Zr) closest to that of the Zr_4Sn (80.0 at % Zr).

5.1.4 Summary of paper IV

Contribution to the study of phase equilibria in Fe-Nb-Zr and preliminary thermodynamic assessment at 800 ºC

R. Jerlerud Pérez and Bo Sundman

The niobium bearing multicomponent zirconium alloy Zirlo (Zr-1Nb-1Sn-0.5Fe), and E-365 (Zr-1.2Sn-0.4Fe-1Nb), represent the new generation of material for fuel cladding and other structural part in the nuclear reactor, due to their better corrosion resistance and irradiation growth compared with Zircaloy-2 and 4. Since the intermetallic compounds in the Fe-Nb-Zr ternary system are also present in the Zr multicomponet alloy and the fact that the composition of these intermetallic phases change during *in- reactor* performace a better knowledge of this ternary system is needed. On the basis of the CALPHAD (CALculation of PHase Diagram) technique, a tentative thermodynamic assessment of the Fe-Nb-Zr ternary system was performed at 800 °C and the optimising module (Parrot) of Thermo-Calc software was used. The thermodynamic models based on the Compound Energy Formalism (CEF) has been used to describe the Gibbs energy of the intermetallic phases stable at 800 °C: Laves_C15, laves_C14, Laves_C36 and the $Fe(Nb,Zr)_2$_Cubic phase. Despite the lack of experimental data it was possible to calculate several

isothermal sections at 800°C and even at 570 °C, 680 °C and 900 ° and to explore the use of the Zr alloys thermodynamic database on industrial applications, for example the effect of oxygen addition to the Fe-Nb-Zr system.

5.1.5 Summary of paper V

Thermodynamic evaluation of the Nb-O-Zr system

R. Jerlerud Pérez and A.R. Massih

The Zr rich Zr-Nb binary alloys are employed in water cooled nuclear reactors in fuel and core components. Due to the fact that these alloys interact strongly with oxygen, which acts as α-stabilizer affecting mainly the α+β→β transition temperature, detailed knowledge of the phase equilibria is important for the manufacturing of the alloys as well as for the material's *in-reactor* performance.

In this paper the thermodynamic description of the O-Nb-Zr ternary system consists of extrapolations from the binary system which means that any ternary excess energies have been evaluated. The accuracy of the extrapolations have been tested and compared with the available experimental data. The phase diagram data in the O-Nb-Zr ternary system are reviewed and presented in Figs. 1-12. The thermodynamic calculations with the Zr alloys database using Thermo-Calc software are presented and include: the binary phase diagram of Nb-Zr, O-Zr and Nb-O, isothermal section at 1273,1473 and 1773 K for the entire ternary system and compared with the experiments, thermodynamic properties of the Nb-O oxides, isoplethal sections for a given oxygen or Nb content in Zr rich ternary alloys, Figs. 13-27. The results indicate that the models describe the zirconium rich portion of the ternary phase diagram satisfactorily. However in the niobium rich part, the calculations differ from the experiments, for example the calculations at 1273 K describe better the phase boundaries between β-Nb+ ZrO_2_monoclinic and α-Zr+β-Nb+ZrO_2_monoclinic than the experimental data which are inconsistent with each other. Moreover the calculated solubility of O in β-Nb phase does not agree with some of the experimental data. It is not clear if the experimental data reported really represent the oxygen content in β-Nb phase or the overall oxygen composition in the two-phase field β-Nb phase+ZrO_2 at some unknown oxygen potential. The calculated Nb rich corner is plotted with logarithmic composition axes and the decrease of oxygen solubility with increasing zirconium content is a straight line, representing the constant solubility product $x_{Zr}.x_O^2 = 2.0.10^{-15}$, determined using the chemical potential of the component for the phases in equilibrium. It was conclude that the calculated results would be verified with new experiments.

Since the thermodynamic assessment of the Nb-O by Dupin *et al.* [90] has not been published, the calculated thermodynamic properties of the oxides in this system were compared with the available experimental information and the agreement was good.

In the review of the experimental data additional information about order-disorder transition temperature in $Nb_{1-x}Zr_xO_2$ is given.

5.1.6 Summary of paper VI

The Sn-Zr Binary System: experiments and thermodynamic assessment

R. Jerlerud Pérez, C. Toffolon_Masclet, J.M.Joubert and B. Sundman

In this paper an experimental study on the Sn-Zr system to conform the theoretical result by first principle calculations presented is presented in paper III. The experiments consist of: X-ray diffraction, EPMA, mass-density and calorimetry measurements and isothermal annealing. The chemical composition of Zr_4Sn phase was determined: at 81.2 at %Zr i.e. non-stoichiometric, at 1273 K and its crystallographic structure was identified as cubic A15 (Cr_3Si prototype). The results indicated that the Zr substitution on the Sn sublattice explained the non-stoichiometry of this phase, two possibilities were studied: vacancies on the Sn sublattice $Zr_3(Sn_{.75}\ Va_{.25})$ and Zr substitution in the Sn sublattice Zr_3 $(Sn_{.8}\ Zr_{.2})$. This conformed the *ab inito* results.

In order to conform the Zr_5Sn_4 and to explore the possibility of a miscibility gap in t the η phase (Zr_5Sn_{3+x} $0 \leq x \leq 1$) below 1100 ºC previously reported, three alloys were annealed at 1273 K for 9 days: 66 at% Zr located on the Zr rich side in the two phase domain $Zr_4Sn+Zr_5Sn_3$, at 59 at. % Zr in the middle of the possible composition range and at 51 at % on the Zr rich side in the two phase domain, $Zr_5Sn_4+ZrSn_2$. The phase η with two composition sets Zr_5Sn_4 (with Ti_5Ga_4 structure) and Zr_5Sn_3 (with Mn_5Si_3 structure) was conformed. The analysis for the alloy with 59 at % Zr indicated the coexistence of the compounds: one richer in Sn, refined at composition $Zr_5Sn_{3.5}$ with larger lattice parameters, one poorer in Sn (Zr_5Sn_3). Our results indicated that the miscibility gap is between Zr_5Sn_3 and $Zr_5Sn_{3.5}$ and not between Zr_5Sn_3 and Zr_5Sn_4 as proposed in the literature. The temperature of the peritectoid reaction β-Zr + $Zr_4Sn \leftrightarrow$ α-Zr was determined at 1216 ±5 K, 40 degrees below the previously reported value.

The reassessment of the Zr-Sn binary system presented in this paper was performed using new experimental information together with previous data and with first principle calculated enthalpies of formation of all the intermetallic compounds in this system. Both theoretical and experimental data could be used within the Compound Energy Formalism (CEF) in order to describe the composition range of the A15 phase and the stability range of the η phase. The η phase was modelled assingle phase including the miscibility gap at low temperature. The liquid, bcc, hcp and were treated as substitutional solutions. The assessment was performed using the Parrot module of the Thermo-Calc software.

References

[1] A.V. Nikulina, V.A. Markelov, M.M. Peregud, V.N. Voevodin, V.L. Panchenko, G.P. Kobylyansky, J. Nucl. Mater. 238 (1996) pp. 205-210.

[2] George P. Sabol, Robert J. Comstock, Robert A. Weiner, Paula Larouere and Robert N. Stanutz.. Zirconium in the Nuclear Industry : 10th International Symposium, ASTM STP 1245, A.M. Garde and E.R. Bradley, Eds., American Society for Testing and Materials, Philadelohia, (1994) pp.724-744

[3] http://www.npp.hu

[4] Y. Etoh, S. Shimada, T. Yasuda, T. Ikeda, R. B. Adamson, J-S Fred Chen, Y. Ishii and K. Takei, Zirconium in the Nuclear Industry : 11th International Symposium, ASTM STP 1295, E.R. Bradley and G.P. Sabol, Eds., American Society for Testing and Materials,(1996) pp. 825-848.

[5] P. Barberis, N. Dupin, C. Lemaignan, A. Pasturel, JM. Grange. Zirconium in the Nuclear Industry, 14th ASTM International Symposium, June 13-17, 2005 Stockholm

[6] G. Ökvist K. Källström, J. Nucl. Mater., 35 (1970) pp. 316.

[7] D. Charquet, E. Alheritiere., Zirconium in the Nuclear Industry, 7th ASTM International Symposium, m ASTM STP 939 Philadelphia, (1987), p. 284

[8] V.N. Shishov, M.M. Peregud, A.V. Nikulina, P.V. Shebaldov, A :V : Tselichev, A.E : Novoselov, G.P. Kobylyansky, Z.E. Ostrovsky and V.K. Shamardi, Zirconium in the Nuclear Industry : 13th International Symposium, ASTM STP 1423, G.D. Moan and P. Rudling., Eds., ASTM International West Conhohocken, PA (2002) pp.758-779.

[9] V.N. Shishov, , A.V. Nikulina, , V. A. Markelov, M.M. Peregud, A.V : Kozlov, S.A. Averin, S. A . Kolbenkov and A. E. Novoselov. Zirconium in the Nuclear Industry : 11th International Symposium, ASTM STP 1295, E.R. Bradley and G.P. Sabol, Eds., American Society for Testing and Materials, (1996) pp.603-622.

[10] S.A. Nikulin, V. I Goncharov, V. A Markelov and V. N. Shishov, Zirconium in the Nuclear Industry : 11th International Symposium, ASTM STP 1295, E.R. Bradley and G.P. Sabol, Eds., American Society for Testing and Materials,(1996) pp.695-709.

[11] C. Ramos, C. Saragovi, M. Granovky and D. Arias, Hyp. Interactions 122 (1999) pp. 201-207.

[12] M.S. Granovsky, M. Canay, E. Lena, D. Arias, J. Nucl. Mater. 302 (2002) pp.1-8.

[13] C. Toffolon, J-C Brachet, C. Servant L. Legras, D. Charquet, P. Barberis adn J-P Mordon, 13th International Symposium, ASTM STP 1423, G.D. Moan and P. Rudling., Eds., ASTM International West Conhohocken, PA (2002) pp.361-383.

[14] C. Ramos, C. Saragovi, M. Granovsky and D. Arias, J. Nucl. Mater, 312 (2003) pp. 266-269

[15] C. Lemaignan and A. Motta, In, Mat. Sc. and Tech., Nuclear Materials, Eds., R.W. Cahn, P. Haasen and E. J. Kramer, 10B, Nuclear Materials, ISBN: 1-56081-882-4 (New york), 1994

[16] M. Griffiths, J.F: Mecke and J.L. Winnegar. Zirconium in the Nuclear Industry, 11th Int. Symp. ASTM STP 1295 A.M. E.R. Bradley and G.P. Sabol Eds., American Society for Testing and Materials, (1996) pp. 508-602

[17] F. Lefebvre and C. Lemaignan, j or Nucl. Mater. 165 (1989) pp. 122.127

[18] M. Griffiths R.W. Gilbert and G.J.C. Carpenter, J of Nucl. Mater. 150 (1987) pp. 53-66

[19] J. A. Faldowsk, A.T. Motta, L. M. Howe and P. M. Okamoto, Mat. Res. Soc. Symp. Proc., 398 (1996), pp. 183-188,
[20] A. T. Motta, L. H. Howe and P.R Okamoto, J. Nucl. Mater., 205 (1993) pp. 258-266.,
[21] D. Pecheur, F. Lefebvre, A.T. Mota C Lemaignan and Charquet.)
[22] AT. Motta, J. of Nucl. Mater., 244 (1997) pp.227-250
[23] F. Garzarolli, W. Goll, A. Seibol and I. Ray. Zirconium in the Nuclear Industry, 11th Int. Symp. ASTM STP 1295 A.M. E.R. Bradley and G.P. Sabol Eds., American Society for Testing and Materials, (1996) pp. 541-556
[24] A. T Motta and Lemaignan, J Nucl. Mater., 195 (1992), pp. 277-285
[25] A. T. Motta and D.R. Olander, Acta Metall. Mater., 38 (1990) pp. 2175-2185
[26] W.L. Bragg and E. G. Willians, Proc. Roy. Soc., A145 (1934) pp. 699
[27] M. Hillert and L.I Staffansosn, Act Che. Scand., 25 (1970) pp. 3618-3626
[28] B. Sundman. and J. Ågren, J. Phys. Chem. Solids, 42. (1981) p. 297
[29] M. Hillert, J of Alloys and Comp,. 320 (2001), pp. 161-176
[30] A. Nikulina, V.N. Shishov, M. M. Peregud, A.V. Tselischev, V.K. Shamardin, G.P Kobylyansky, Effect of Irradiation on Materials:18th Internatinal Symposium, ASTM STP 1325, R.K. Nanstad, M.L. Hamilton, F.A. Garner and A.S: Kumar, Eds, American Society for Testing and Materials (1999) pp. 1045-1061
[31] H. Anada, B. J. Herb, K-I Nomoto, S. Hagi, R.A. Graham and T. Kuroda. Zirconium in the Nuclear Industry : 11th International Symposium, ASTM STP 1295, E.R. Bradley and G.P. Sabol, Eds., American Society for Testing and Materials,(1996) pp.74-91
[32] D. Pecheur, F. Lefebvre, A.T. Motta and C. Lemaignan, J.F. Wadier., J. Nucl. Mater., 189, (1992) pp. 318-332
[33] G.M. Hood., J Nuclear Materials, 159 (1988) pp. 149-175
[34] M Griffits, R-A, Holt and A. Rogerson, J. of Nucl. Mater., 225 (1995), 245-248
[35] D.J.n Bacon, J. Nucl. Mater., 206 (1993)] pp. 249-265
[36] D.G. Westalake, J Nucl. Mater., 26, 2 (1968) pp. 208-216
[37] F. Garzarolli R. Schumann and E. Steinberg. Proc. 10th Int. Symp. On Zr in the Nuclear Industry, Boltimore, MD, ASTM-STP-1245 (1994) pp. 709-723]
[38] Rudling and B. Lehtinen, Electric Power Research Inst., Palo Alto, CA, report EPRI-TR 03396 (1993),
[39] Rudling, M. Lindbäck, B. Lethinen, H.-O. Andrén and K Stiller, Zr in the Nuclear Industry, 10th Int. Symp. ASTM STP 1245 A.M. Garde and E.R. Bradley Eds., American Society for Testing and Materials, West Conshohocken PA, (1994) pp. 599-614,
[40] H. Anada, K. Nomoto and Y. Shida on Zr in the Nuclear Industry, 10th Int. Symp. ASTM STP 1245 A.M. Garde and E.R. Bradley Eds., American Society for Testing and Materials, West Conshohocken PA, (1994) pp. 307-327.
[41] D. Charquet, J of Nucl. Mater., 211 (1994) pp. 259-261
[42] R. J. Comstock, G. Schoenberger and G.P. Sabol. Zr in the Nuclear Industry, 10th Int. Symp. ASTM STP 1245 A.M. Garde and E.R. Bradley Eds., American Society for Testing and Materials, West Conshohocken PA, (1994) pp. 710-725
[43] D. Charquet., J. Nucl. Mater. 288 (2001) pp. 237-240
[44] Y . de Carlan, C. Regnard, M. Griffiths, D. Gilbon and C. Lemaignan. Zirconium in the Nuclear Industry, 11th International Symposium, ASTM STP 1295, E.R. Bradley and G.P. Sabol, Eds., American Society for Testing and Materials,(1996) pp.638-653
[45] T.R.G. Kutty, R. Ravi and C Ganguly, J. Nucl. Mater. 265 (1999) pp.91-99

[46] L. Kaufman and Bernstein, Computer Calculation of Phase Diagrams, Academic Press, New York,1970.

[47] N. Saunders and A.P. Miodownik CALPHAD-Calculation of phase diagrams, Pergamon Materials Series vol. 1 ed. R.W: Cahn, elsevier Science:Oxford, 1998

[48] N. Saunders. Proceeding, 9th In ternational Conference on Aluminium Alloys, Brisbane, Australia,2-5 august, 2004

[49] K. Frisk and M. Selleby. J of Alloys and Comp., 320 (2001), 177-188.

[50] N. Saunders, in Superalloys 1996, eds. R.D. Kssinger *et al.* TMS, Warrendale, 1996, 101

[51] B. Sundman. and J. Ågren, , J. Phys. Chem. Solids 4, 2 (1981) pp. 297

[52] B. Sundman, Calphad J., 8 (1984) pp. 104

[53] A.T Dinsdale, Calphad, 15, 4 (1991), 317

[54] M. Hillert and M. Jarl, Calphad 2 (1978). pp.227-238

[55] G. Inden, Physica, 10B (1981) pp. 82-10

[56] M. Hillert, B. Jonsson, B- Sundman and J. Ågren, Met. Trans. A, 16A (1984) pp.261-266

[57] M. Hillert, Bull. Of Alloy Phase Diagram, 2, 3 (1983) pp. 265-268

[58] B. Johsson, TRITA- MAC-0233, Materials Center, Royal Institute of Technology, Sweden 1984.

[59] M. Jacobs, private communication.

[60] L. Kaufman, P.E.A. Turchi, W. Huang and Zi-Kui-Liu, Calphad, 5, 3 (2001) pp.419-433.

[61] P.A. Korzhavyi, Bo Sundman, Malin Selleby and B. Johansson, Mater. Res. Soc. Proc., 842 (2005) 24.10.1

[62] F. de Boer, R. Boom, W.C.M. Mattens, A.R. Miedema, A.K. Niessen, Cohesion in Metals, vol 1 D.G. Pettifor Eds, , North_Holland 1989.

[63] J. R. Chelikowsky, Phys Rewiew B, 5, 10 (1982) pp. 6506.

[64] G. S. Collins and M. O. Sacate, Hyperfine interactions, (2004) pp. 1

[65] Q. Guo and O. J. Kleppa, Met. and Mater. Transactions B, 29B (1998) pp. 815.

[66] A. Fernández Guillermet, J. Alloys and Compounds, 217 (1995) pp. 69-89

[67] R. Jerlerud. Perez, Calphad, 25, 1 (2001) pp.59-66

[68] J-O Andersson, B. Sundman, Calphad, 11 (1987) p 83-92

[69] J. Costa Neto, S. G. Fries, H.L. Lukas, Calphad 17, 3 (1993) pp. 219-28

[70] A. Dinsdale, T. Chart, MTDS NPL, Unpublished work (1986)

[71] K. Zeng, M. Hamalainen, and I. Ansara, Z. Metallkde. 84 (1993) 23-28.

[72] C. Toffolon and C. Servant, Calphad, 24, 2 (2000) pp.97.112

[73] K.C Hari Kumar, P Wollannt and L Delay, Calphad, 20, 2 (1996) pp.139-149

[74] C Servant., C. Gueneau, I. Ansara J. Alloys and Compounds, 220, 1-2 (1995) pp.19-26

[75] G. Ghosh, Unpublished Research, Northwestern University, 1998, privat communication

[76] N. Sauders Calphad, 9, 4 (1985) pp. 297309

[77] R. Jerlerud Pérez, Calphad 27 (2003) pp. 253-262

[78] Frisk, Calphad 14 (1990), pp. 311-320

[79] C. Vahlas, P.Y. Chevalier and E. Blanquet, Calphad, 13 (1989) pp. 273-292

[80] C. Toffolon, C. Servant, J.C. Gachon, B. Sundman, J of Phase Eq., 23, 2 (2002) pp.134-139

[81] A.Fernandez Guillermet, Z. Metallkde., 82 (1991) p.478-487
[82] C. Gueneau, C. Servant, I. Ansara, and N. Dupin, Calphad, 18, 3 (1994) pp. 319-328
[83] R. R. Jerlerud Pérez, C. Toffolon-Masclet, JM. Joubert and B. Sundman, to be published
[84] R. Jerlerud Pérez and B. Sundman, provisional Fe-Nb-Zr, 2006
[85] I. Ansara, N. Dupin, J.M. Joubert, M. Latorche and Percheron-Guegan, J. of phase equilibria, 19, 1 (1998) pp.6-10
[86] J R Taylor and A T Dinsdale, Z Metallkde, 81 (1990) pp. 354-366
[87] J R Taylor and A T Dinsdale, Z Metallkde, 84 (1993) pp.335-345
[88] B Sundman, J. Phase Eq. 12 (1991) pp. 127-140
[89] R Luoma, Calphad 19 (1995) pp. 279-295
[90] N. Dupin, I. Ansara, C. Servant, C. Toffolon, C. Lemaignan, J C Brachet. J . of Nucl. Mater. 275, 3 (1999) pp. 287-295. Also in (http://www.inpg.fr/ltpcm/base/zircobase)
[91] P. Liang, N. Dupin, S.G. Fries, H.J. Seifert, I. Ansara, H.L. Lukas, F. Aldinger, Z. Metallkunde (2001) pp. 747-756
[92] B J Lee, Calphad 17, 3 (1993) pp. 251-268
[93] N. Dupin and I. Ansara, Z. Metallkde., 87, 7 (1996) pp.555-561
[94] M. Kowalski and P.J. Spencer, Calphad 19 (1995) 229-243
[95] J-M. Joubert, M. Latroche, A. Percheron-Guйgan and I. Ansara, J. Phase Equilibria, 16, 6 (1995) 485-492.
[96] F. Stein, G. Sauthoff and M. Palm, J. of Phase Equilibria, 23, 6 (2002) pp. 480-494
[97] C. Toffolon-Masclet, S. Chatain, C. Gueneau and N. Dupin, Calphad XXXIV, May 22-27,2005, Maastricht, The Netherlands.
[98] R. Jerelrud Pérez, A. Massih, to be published
[99] S.F. Aricó, L.M. Gribaudo, L.A. Roberti, J of Materials Science, 31 (1996) pp. 5587-5591
[100] S.F. Aricó and L.M. Gribaudo, Scripta Mater., 41, 2 (1999) pp 159-165
[101] Y-U. Kwon, and J.D.Corbett, Chem. Mat., 4, 6 (1992) pp.187-190.
[102] Zirconium in the Nuclear Industry, 11th Int. Symp. ASTM STP 1295 A.M. E.R. Bradley and G.P. Sabol Eds., American Society for Testing and Materials, (1996) pp. 638-651
[103] M. Hillert, Phase Equilibria and Phase Transformation, Their Thermodynamic Basis, Cambridge University Press, 1998
[104] R. Hirschl, J. Hafner and Y. Jeanvoine., J. Phys: Condens. Matter. 13 (2001) pp. 3545-3572

Appendix 1

SYSTEM **REFERENCE**

FE-SN-ZR

60Tan TANNER. SYSTEME ZR-FE-SN.
TRANS. AMER. SOC. MET., 1960, 52, 1115-32. FE-SN-ZR

58Tan TANNER L.E./LE SYSTEME ZR-FE-SN.
STATUS REPORT, JULY 1957,MAR. 1958, 4.
FE-SN-ZR

62Ten TENNER L.E./LEVINSON D.W., STRUCTURES IN THE
ZIRCONIUM-IRON-TIN SYSTEM. U.S. AT ENERGY
COMM.TID.7625, 1962, 30-41. FE-SN-ZR

90Kor KOROTKOVA N.V.,LE COIN RICHE EN ZR DU DIAGRAMME DE
PHASES DU SYSTEME ZR- SN- FE.
IZVEST.AKAD.NAUK SSSR, METALLY, 1990, (5), 206-213.
FE-SN-ZR

ZIRCONIUM CORNER OF THE ZR-SN-FE PHASE DIAGRAM .
KOROTKOVA N.V./
RUSS.METALL., 1990, (5), 201-208. MET.ABSTR., 24-11-0960.
FE-SN-ZR

98Mel MELNYK G.A./FRUCHART D./ROMAKA L.P./STADNYK
J.V./SKOLOZDRA R.V./
CRYSTAL STRUCTURE OF NEW M'6M"(1.5+X)X(1.5-X)
COMPOUNDS (M4=ZR, HF;M"=FE, CO, NI; X = SN, SB) AND
ELECTRONIC STRUCTURE OF ZR6CO1.65SN1.35.
J. ALLOYS COMPD., 267, (1-2) L1-L3 (1998).
FE-SN-ZR CO-SN-ZR NI-SN-ZR CO-SN-ZR FE-HF-SN CO-HF-SN
HF-NI-SNFE-SB-ZR CO-SB-ZR NI-SB-ZR FE-HF-SB CO-HF-SB
HF-NI-SB

CR-FE-ZR

62Sve SVECHNIKOV V.M./SPEKOV A.TS.
CONSTITUTION DIAGRAM OF THE ZRCR2-ZRFE2 SYSTEM.
SB.NAUCHN.TR.METAL.,AKAD.NAUK.UKR.SSSR., 1962, 16,
145-52.
CR-FE-ZR

79Mal MALAKHOVA. T.C. STUDY OF PHASE DIAGRAMS OF THE
ZIRCONIUM PART OF THE ZIRCONIUM-CHROMIUM-IRON, AND
ZIRCONIUM-CHROMIUM-COPPER SYSTEMS . SPLAVY AT.ENERG.,
1979, 123-130.
FE-ZR CR-FE-ZR CR-CU-ZR

86Yin MENG XIAN YING./NORTHWOOD D.O.POLYTYPE STRUCTURES IN
ZRCRFE LAVES PHASE .DEPT.ENG.MATER., UNIV. WINDSOR,
WINDSOR, ONTARIO N9B 3P4, CANADA. J.LESS COMMON MET.,
1986, 125, 33-44.

CR-FE-ZR

95Sou SOUBEYROUX J.L./BOUOUDINA M./FRUCHART D./PONTONNIER L./
PHASE STABILITY AND NEUTRON DIFFRACTION STUDIES OF LAVES PHASES ZR(CR(1-X)M(X))2 WITH M=MN, FE, CO, NI, CU AND 0<X<0.2 AND THEIR HYDRIDES.
J.ALLOYS COMPDS., 219, (1-2), 48-54 (1995).
CR-MN-ZR CR-FE-ZR CO-CR-ZR CR-CU-ZR CR-H-MN-ZR CR-FE-H-ZB CO-CR-H-ZR CR-CU-H-ZR

FE-NI-ZR

73Tar TARARAEVA E.M./IVANOV O.S./REFINEMENT OF THE PHASE DIAGRAM OF THE ZIRCONIUM-IRON-NICKEL SYSTEM . .
STR.SVOISTVA SPLAVOV DLYA AT.ENERG., 1973, 131-138.
FROM REF.ZH., TEPLOENERG. 1973, ABSTR. N. 12U203.
FE-NI-ZR

90Sid SIDOROV O.YU./VALISHEV M.G./PLETNEVA E.D./ESIN YU.D./GELD P.V./
ENTHALPIE DE FORMATION D'ALLIAGES LIQUIDES TERNAIRES A BASE
DE NI. ZH.PRIKL.KHIM., 1990, 63, (7), 1497-1501.
FE-NI-Y CO-NI-Y CU-NI-Y CU-NI-ZR FE-NI-ZR CO-NI-ZR

93Wan WANG H./LUCK R./PREDEL B.,THERMODYNAMIC INVESTIGATION ON LIQUID IRON-NICKEL-ZIRCONIUM ALLOYS.
J. PHASE EQUIL., 14, 1, 22-30, 1993. FE-NI-ZR

NB-SN-ZR

73Tar TARARAEVA E.M./MURAV'EVA L.S./IVANOV O.S./
STRUCTURE OF THE QUATERNARY ZIRCONIUM-NIOBIUM-TIN-OXYGEN SYSTEM PHASE DIAGRAM AND ITS BOUNDING TERNARY DIAGRAMS .
STR.SVOISTVA SPLAVOV DLYA AT.ENERG., 1973, 138-143.
FROM REF.ZH.,TEPLOENERG. 1973, ABSTR. N. 12U207.
NB-O-SN-ZR NB-O-SN NB-O-ZR O-SN-ZR NB-SN-ZR

74Sob SOBOLEVA N.G./SOKOLOVSKAYA E.M./AGAFONOV V.N./FEDOROVA M.A./
PHYSICAL-CHEMICAL STUDY OF THE TERNARY SYSTEM NIOBIUM-ZIRCONIUM-TIN . 149-152 PP. STRUKTURA FAZ, FAZOVYE PREVRASHCHENIYA DIAGRAMMY SOSTOYANIYA METALL.SISTEM., IVANOV O.S. (ED.), MOSCOW; IZDATEL'STVO
NAUKA (1974). (IN RUSSIAN). SEE CONF-7209120. N.S.A. 31-12032.NB-SN-ZR

90Kor KOROTKOVA N.V., EQUILIBRE DE PHASES DANS LE SYSTEME ZR- NB- SN
IZVEST.AKAD.NAUK SSSR, METALLY, 1990, (4), 202-208.
NB-SN-ZR----------transl
PHASE EQUILIBRIUM IN THE ZR-NB-SN SYSTEM
KOROTKOVA N.V./
RUSS.METALL., 1990, (4), 207-213.
MET.ABSTRE., 24-11-0881.
NB-SN-ZR

96Can CANAY M./ARIAS D.,TRANSFORMATION TEMPERATURES AND STRUCTURE OF ZIRCONIUM-TIN-NIOBIUM ALLOYS. AN.ASOC.QUIM.ARGENT., 84, (4), 343-347 (1996). NB-SN-ZR

O-SN-ZR

73Tar TARARAEVA E.M./MURAV'EVA L.S./IVANOV O.S./ STRUCTURE OF THE QUATERNARY ZIRCONIUM-NIOBIUM-TIN-OXYGEN SYSTEM PHASE DIAGRAM AND ITS BOUNDING TERNARY DIAGRAMS . STR.SVOISTVA SPLAVOV DLYA AT.ENERG., 1973, 138-143. FROM REF.ZH.,TEPLOENERG. 1973, ABSTR. N. 12U207. NB-O-SN-ZR NB-O-SN NB-O-ZR O-SN-ZR NB-SN-ZR

92Kwo KWON Y.U./CORBETT J.D./INFLUENCE OF OXYGEN ON THE STABILITY OF ZIRCONIUM-TIN (ZR4SN), DEP.CHEM., IOWA STATE UNIV., AMES, IA 50011 USA. CHEM.MATER., 1992, 4, (1), 187-190. O-SN-ZR

95Tsu TSUJI TOSHIHIDE/AMAYA MASAKI/NAITO KEIJI/HEAT CAPACITY MEASUREMENT ON (ZR(1-Y)M(Y))OX (WHERE M IS NB, SN) FROM 325 TO 905 K. THERMOCHIM.ACTA, 253, 19-31 (1995). NB-O-ZR O-SN-ZR

96Ari ARICO S.F./GRIBAUDO L.M./ROBERTI L.A./ EQUILIBRIUM PHASES SURROUNDING THE ALPHA-ZR SOLID SOLUTION IN THE ZR-SN-O SYSTEM. J.MATER.SCI., 31 (21), 5587-5591 (1996). O-SN-ZR

NB-O-ZR

73Tar TARARAEVA E.M./MURAV'EVA L.S./IVANOV O.S. STRUCTURE OF THE QUATERNARY ZIRCONIUM-NIOBIUM-TIN-OXYGEN SYSTEM PHASE DIAGRAM AND ITS BOUNDING TERNARY DIAGRAMS . TR.SVOISTVA SPLAVOV DLYA AT.ENERG., 1973, 138-143. FROM REF.ZH.,TEPLOENERG. 1973, ABSTR. N. 12U207. NB-O-SN-ZR NB-O-SN NB-O-ZR O-SN-ZR NB-SN-ZR

74Ort ORTALI P.L./JEHN H./LIMITE DE SOLUBILITE DE O DANS LA PHASE SOLIDE D'ALLIAGES NB-ZR RICHES EN NB LAB.TECNOL.MATER.MET. NON TRADIZIONALI, C.N.R., CINISELLO B., MILANO,ITALIE. METALLURG.ITAL., ITAL., 1974, 66, (5), 263-266. NB-O-ZR.

74Jeh JEHN H./ORTALI P. SOLUBILITE DE O ET CINETIQUE DE L'ABSORPTION DE O DANS D'ALLIAGES NB-ZR RICHES EN NB . Z.METALLKDE., 1974, BD.65, H.9, P.586-592. NB-O-ZR

79Rin2 RINEHART G.H. HIGH TEMPERATURE THERMODYNAMICS AND VAPORIZATION OF THE ZIRCONIUM-NIOBIUMOXYGEN SYSTEM . UNIV. KANSAS, LAWRENCE, KANSAS, USA. AVAIL.UNIV,MICROFILMS INT., ORDER N. 7910582. 410 PP. (ENG.). FROM DISS.ABSTR.INT.B, 1979, 39, (11), 5397. NB-O-ZR.

81Nak NAKAI K./KINOSHITA C./KITAJIMA S./EFFECTS OF OXYGEN AND/OR NITROGEN ON PHASE TRANSFORMATIONS ABOVE THE MONOTECTOID TEMPERATURE IN NB-ZR ALLOYS . DEPT.NUCL.ENG.FAC.ENG. KYUSHU UNIV. FUKUOKA 812, JAPAN. J.NUCL.MATER., 1981, 98, 131-143. N-NB-ZR NB-O-ZR.

82Set SETA KATSUO./NAITO KEIJI. CALORIMETRIC STUDY OF THE PHASE TRANSITION IN DOPED NBO2 DEPT.NUCLEAR ENG., FAC.ENG., NAGOYA UNIV., FURO-CHO, CHIKUSA-KU, NAGOYA 464, JAPAN. J.CHEM.THERMODYNAMICS, 1982, 14, (10), 937-949. NB-O-ZR MO-NB-O.

86Asu ASUNDI M.K./GARG S.P./MUKHOPADHYAY P./TIWARI G.P./SAROJA A./ THE NIOBIUM-OXYGEN-ZIRCONIUM SYSTEM . PHYS.METAL.DIV., BHABHA ATOMIC RES.CENT., TROMBAY, BOMBAY-400 085, INDIA. J.ALLOY PHASE DIAGRAMS, 1986, 2, (2), 141-148. NB-O-ZR.

89Per PERELYAEV V.A./MIROSHNIKOVA L.D./ALYAMOVSKII S.I./KELLERMAN D.G., FORMATION DES PHASES DANS LES SYSTEMES NBO- TAO, NBO- ZRO ET NBO2-TAO2 . ZH.NEORG.KHIM., 1989, 34, (3), 750-753. NB-O-TA NB-O-ZR

89Aly ALYAMOVSKII S.I./MIROSHNIKOVA L.D./PERELYAEV V.A./FEDYUKOV A.S./ FORMATION DES PHASES DANS LES SYSTEMES PARTIELS NBO-TAO, NBO2- TAO2 ET NBO- ZRO DANS CERTAINES CONDITIONS DE T ET PRESSION . ZH.NEORG.KHIM., 1989, 34, (5), 1281-1284. NB-O-TA NB-O-ZR

92Bal BALABAEVA R.F./VASILEVA I.A./SUKHUSHINA I.S./ ENTHALPIE ET ENTROPIE PARTIELLES DE O DANS LES ALLIAGES DE V ET NB AVEC DE FAIBLES TENEURS DE METAUX DE TRANSITION ET DE O ZH.FIZ.KHIM., 1992, 66, (3), 803-806. O-SC-V O-TI-V CR-O-V MN-O-V FE-O-V O-V-Y O-V-ZR NB-O-V MO-O-V O-TC-V LA-O-V HF-O-V O-TA-V O-V-W NB-O-SC NB-O-TI NB-O-V CR-NB-O MN-NB-O FE-NB-O NB-O-Y NB-O-ZR MO-NB-O NB-O-TC LA-NB-O HF-NB-O NB-O-TA NB-O-W.

92Tsu TSUJI T./AMAYA M./NAITO K./ HEAT CAPACITY MEASUREMENT OF ZIRCONIUM ALLOY (ZROX) AND ZIRCONIUM NIOBIUM ALLOY ((ZR1-YNBY)OX) FROM 325 TO 905 K. J.THERM.ANAL., 38, 8, 1817-1826 (1992)O-ZR NB-O-ZR.

93Mag MAGUNOV R.L./SOTULOV V.S./MAGUNOV I.R./ RELATIONS DE PHASES DANS ZRO2(HFO2)-NB2O5. ZH.NEORG.KHIM., 38, 2, 357-362 (1993). HF-NB-O NB-O-ZR.

93Pog MAGUNOV R.L

PHASE RELATIONS IN THE ZIRCONIUM DIOXIDE (HAFNIUM DIOXIDE)-NIOBIUM PENTOXIDE SYSTEMS.
ZH.NEORG.KHIM., 38, (2), 363-365 (1993).
abs .C.A. 118-241932R.
NB-O-ZR HF-O-ZR

96Asu ASUNDI, MK; GARG, SP; MUKHOPADHYAY, P; TIWARI, GP; SAROJA, A
THE NIOBIUM--OXYGEN-ZIRCONIUM SYSTEM
J. ALLOY PHASE DIAGRAMS, VOL. 2, NO. 2, PP. 141-148, MAY 1986.

73Tar TARARAEVA, E.M./ MURAVEVA, L.S./IVANOV, O.S.
STRUCTURE OF THE QUATERNARY PHASE DIAGRAM OF THE ZR-NB-SN-O SYSTEM AND ITS TERNARY BOUNDARIES.
STROENIE SVOISTVA SPLAVOV DLYA ATOM. ENERG., NAUKA, MOSCOW, 1973, 138-143

71Shu SHURIN, A.K./ LOKTIONOV, V.A.
PHASE EQUILIBRIA IN NB-O-HF AND NB-O-ZR ALLOYS
DIAGRAMMY SOSTOYANIYA METAL. SISTEM NAUKA, MOSCOW, 1971, 82-87.

95Tsu TSUJI TOSHIHIDE/AMAYA MASAKI/NAITO KEIJI
HEAT CAPACITY MEASUREMENT ON (ZR(1-Y)M(Y))OX (WHERE M IS NB, SN) FROM 325 TO 905 K.THERMOCHIM.ACTA, 253, 19-31 (1995).C.A. 122-323511Z. NB-O-ZR O-SN-ZR

FE-O-ZR

74Fru FRUEHAN R.J. THE EFFECT OF ZIRCONIUM, CERIUM, AND LANTHANUM ON THE SOLUBILITY OF OXYGEN IN LIQUID IRON .
RES.LAB., U.S.STEEL CORP., MONROEVILLE, PENNSYLVANIA 15146, USA.
MET.TRANS., 1974, 5, (2), 345-347.
CE-FE-O FE-O-ZR FE-LA-O

76Jan JANKE D./FISCHER W.A.
EQUILIBRES DE DESOXYDATION DU TI, DE AL ET DU ZR DANS BAINS DE FE A 1600 DEG.C
ARCH.EISENHUTTENWES, 1976, 47, N.4, AVRIL, P.195-198.
FE-O-TI AL-FE-O FE-O-ZR

87Alt ALTOUNIAN Z./BATALLA E./STROM-OLSEN J.O./WALTER J.L.
THE INFLUENCE OF OXYGEN AND OTHER IMPURITIES ON THE CRYSTALLIZATION OF NICKEL-ZIRCONIUM (NIZR2) AND RELATED METALLIC GLASSES .
RUTHERFORD PHYS.BUILD., MCGILL UNIV., MONTREAL, PQ CANADA H3A 2T8.
J.APPL.PHYS., 1987, 61, (1), 149-155.
NI-O-ZR FE-O-ZR CO-O-ZR HF-NI-O

87Kim KIMINAMI R.H.G.A.
STUDY OF THE ZIRCONIA-IRON(II) OXIDE-IRON(III) OXIDE SYSTEM BY THERMOGRAVIMETRY AT AIR OXYGEN PARTIAL PRESSURE AND TEMPERATURES UP TO 1500 DEG.C .

UNIV.FED.PARAIBA, 58100 CAMPINA GRANDE, BRAZIL.
CERAMICA (SAO PAULO), 1987, 33, (213), 207-209.
C.A. 108-157159E.
FE-O-ZR.

88Kim KIMINAMI R.H.G.A.
PHASE EQUILIBRIA IN THE ZIRCONIA-FERROUS OXIDE-FERRIC OXIDE SYSTEM AT OXYGEN PRESSURE 2.10(-3) ATM.
DEP.ENG.QUIM., UNIV. FED.PARAIBA, 58100 CAMPINA GRANDE, BRAZIL.
CERAMICA (SAO PAULO), 1988, 34, (223), 121-123.
FE-O-ZR

96Pop POPOVIC S./GRZETA B./STEFANIC G./CZAKO-NAGY I./MUSIC S.
STRUCTURAL PROPERTIES OF THE SYSTEM (M)-ZRO2-(ALPHA)-FE2O3.
J.ALLOYS COMPDS., 241, (1-2), 10-15 (1996).
FE-O-ZR.

97Gua LI GUANGQIANG/SUITO HIDEAKI.
ELECTROCHEMICAL MEASUREMENT OF CRITICAL SUPERSATURATION OF FE-O-M (M=AL, SI, AND ZR) AND FE-O-AL-M (M = C, MN, CR, SI, AND TI) MELTS BY SOLID ELECTROLYTE GALVANIC CELL.
ISIJ INT. (INST OF STEEL AND IRON OF JAPAN)., 37, (8), 762-769 (1997).
abs C.A. 127-321244U.
AL-FE-O FE-O-SI FE-O-ZR AL-C-FE-O AL-FE-MN-O AL-CR-FE-O AL-FE-O-SI AL-FE-O-TI.

98Zav ZAVALIY I.YU./RIABOV A.B./YARTYS V.A./WIESINGER G./MICHOR H./HILSCHER.G.
(HF, ZR)2FE AND ZR4FE2O(0.6) COMPOUNDS AND THEIR HYDRIDES: PHASE EQUILIBRIA, CRYSTAL STRUCTURE AND MAGNETIC PROPERTIES.
J. ALLOYS AND COMPOUNDS, 265, (1-2), 6-14 (1998).
FE-H-HF-ZR FE-HF-ZR FE-O-ZR FE-H-O-ZR

04Hua WEIMING HUANG, OXYGEN SOLUBILITY IN FE-ZR-O, CALPHAD J, 28,
153-157, 2004.